UNIVERSITY OF KANSAS

Department of Chemistry Honors Thesis

A Comprehensive Investigation of Mercaptoazulenes & Their Complexes with Monovalent Gold

Bryce Tappan

Principal Investigator, Mentor, and Committee Chair:

Dr. Mikhail V. Barybin

Committee Members:

Dr. Mikhail V. Barybin _____

Dr. Cindy L. Berrie _____

Dr. Timothy A. Jackson _____

Defended May 13th, 2016

Acknowledgements:

First and foremost, I would like to thank the University of Kansas Chemistry Department as a whole. In my four years at KU, my classes through the Chemistry Department have been consistently rigorous, superbly taught, and have maintained an excellent balance of breadth and depth. Between the quality of the courses, and the opportunity to do undergraduate research, the KU Chemistry Department has provided me with an undergraduate experience surpassed by few institutions, if any, in the country. I certainly believe that I would not have had such a well-rounded, enriching experience as a chemistry undergraduate at any other university. I would like to personally thank Deanne Arensberg, who is the friendly face of the Department of Chemistry for so many undergraduates like me. She made me feel welcome as a Chemistry major from the moment I first walked into her office.

I would also like to express my gratitude for the financial support I have received for several semesters of research through KU's Center for Undergraduate Research and the KU Chemistry Department. Several UGRAs and Departmental Awards allowed me to spend more time in the lab than would have been otherwise possible.

I owe many thanks to Dr. Cindy Berrie and Dr. Timothy Jackson as well. Both have provided me with valuable insights into my own research over the years and kindly agreed to preside on my committee for the defense of this thesis. I admire both of these individuals for their remarkable talent and love of teaching. Dr. Jackson – thank you for graciously tolerating my frequent, spur-the-moment visits to your office which varied in subject matter from troubleshooting problems in research, to application processes, to life in general.

Many thanks to Dr. Andrew Spaeth, Jason Applegate, Nate Erickson, Mason Hart, Moni Okeowo, and Dr. Toshinori Nakakita for guiding me through the painstaking process of becoming a sound synthetic chemist. You all act together to form an encouraging, intellectual, and friendly environment that I have had the privilege of enjoying with you. My love of research at KU stems from the group dynamics of our inorganic family as much as it stems from the chemistry itself. I appreciate the time you have taken to extend your knowledge and friendship to me.

Finally, I cannot thank Dr. Misha Barybin enough for all he has done for me in my time at the University of Kansas. From the day I first stepped onto campus, Misha has mentored and advised me in academics, research, and in life. He enabled me and encouraged me in all that I do. Misha is worthy of admiration for his brilliance as a chemist, a colleague, an advisor, and as an instructor. However, I am always most struck by his endless compassion and consideration for others. I am so honored to have been able to spend my time at KU in the Barybin Group and to have befriended Misha. Thank you.

-Bryce Tappan

Abstract:

Discussed herein are the syntheses and characterization of a family of azulenylthiolate gold(I) complexes, which show promise for applications in the fields of molecular electronics and luminescent chemosensing. The reactivities and the photoluminescent behavior of these systems were investigated via ^{1}H NMR, electronic absorption, fluorescence, and phosphorescence spectroscopies. In addition, single-crystal X-ray crystallography was employed to reveal key structural features of several of the mercaptoazulene ligands and azulenylthiolate gold(I) complexes to provide insight into the origins of these species' unique physicochemical properties. TD-DFT calculations were performed to aid in the interpretation of electronic absorption and photoluminescence spectra. Finally, although not central to advancing the knowledge of these systems, this thesis also provides a complete description of experimental pitfalls that one may need to avoid in attempting to synthesize and characterize such complexes.

Table of Contents

List of All Figures:

Chapter 1:

Introduction to the Gold-Thiolate Motif, Azulene, & Azulenylthiolate Adducts of Gold(I)

1.1 Introduction to the Gold-Thiolate Motif

1.1a *Characteristics of the Gold-Thiolate Bond & Its Use in Molecular Electronics*

Over the last several decades, the gold-thiolate motif has played a central role in the development of a number of emerging fields of chemistry. These systems have spurred great interest due to their potential applications in molecular electronics, luminescent chemosensing, catalysis, the pharmaceutical industry, and drug delivery systems.[1-3] The ensuing discussion will provide a brief introduction to the intriguing properties that motivate much of gold-thiolate research.

While gold is often thought of as being chemically inert, it can assume oxidation states from –I to +V, giving it the ability to form a number of different types of coordination complexes.[1] With a ground-state electron configuration of $[Xe]4f^{14}5d^{10}6s^{1}$, the most common oxidation state of gold is gold(I), which yields a stable, entirely filled outermost $5d^{10}$ atomic orbital. Due to its empty 6s orbital, gold(I) most often coordinates in a linear fashion to two ligands, allowing the ligands to fill the otherwise empty 6s orbital. Organic ligands containing a thiol, or mercapto, group (R-SH) may be deprotonated to produce a thiolate (RS^{-}), which can effectively bond to gold. While all of the thiolate-noble metal bonds exhibit some degree of covalency, the gold-thiolate bond is the most covalent, with the covalent bond between gold and sulfur being similar in strength to that of Au-Au bonds in metallic gold.[1]

The high degree of covalency of the Au-S bond allows sulfur to act as a stable junction between gold and organic ligands, enabling thiolate-mediated electronic communication between gold centers or surfaces and organic frameworks.[1] 1,4-benzenedithiol (BDT) has been the pioneering example of an organic dithiolate that has been shown to conduct electrons between gold

electrodes.[4] The qualities of BDT that make it a sound starting point for molecular electronics applications include its ability to connect two metal electrodes through its two thiolate termini and its planar, conjugated π-system that facilitates the conductance of delocalized electrons from one electrode to the other.

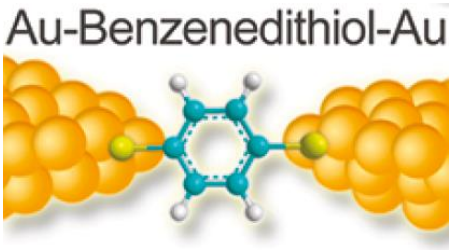

Figure 1.1a: Depiction of 1,4-BDT as molecular conductor between gold electrodes.[4]

1.1b *Luminescence of Gold-Thiolates & the Significance of Aurophilicity*

Apart from their intriguing properties for use in molecular electronics, gold-thiolate systems have drawn attention for their potential applications in luminescent chemosensing. These systems frequently exhibit unique photoluminescence profiles as they often have numerous radiative relaxation pathways. Such pathways include possible ligand-to-metal charge transfers (LMCT), ligand-to-ligand charge transfers (LLCT), metal-to-ligand charge transfers (MLCT), intraligand charge transfers (ILCT), and metal-centered transitions (MC).

Additionally, complexes containing gold(I) often feature intermolecular and intramolecular (for complexes with multiple gold(I) centers) aurophilic effects. This effect, coined aurophilicity, is the formation of weak attractive interactions between separate gold(I) centers. The interaction is similar in strength to that of a hydrogen bond, and arises from the influence of relativistic effects on the atomic orbitals of gold.[6] Relativistic effects cause the s and p orbitals to contract, which consequentially leads to the expansion of the d and f orbitals as the positive charge of the nucleus is more effectively shielded by the electrons within the s and p orbitals. Although

relativistic effects are present in all atomic species, the contraction of the s orbitals, and hence the expansion of the d orbitals, is more prevalent in heavy metals and is most pronounced in gold. The nature of the aurophilic attraction has been attributed to electrostatic interactions, similar to van der Waals forces, only stronger.[1,3,6,] These attractive forces can cause compounds containing gold(I) to oligomerize through the formation of Au···Au aurophilic interactions.

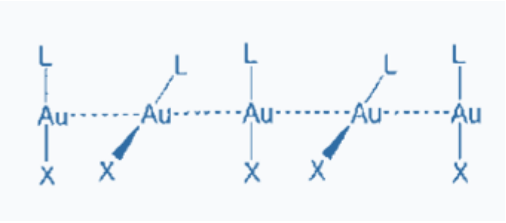

Figure 1.1b: One possible oligomer structure arising from Au···Au interactions.[6]

In fact, oligomerization of complexes featuring gold(I) centers can give rise to yet another charge transfer relaxation pathway, namely, ligand-to-metal-metal charge transfers (LMMCT). The role of aurophilic interactions in facilitating this relaxation pathway is not entirely understood, but it is known that the gold centers associated through aurophilic interactions act as an electron-accepting aggregate.[3,5] Because aurophilic interactions are common in complexes containing sterically unencumbered gold(I) centers, consideration of their effects is crucial for sound interpretation of their luminescent behavior and crystallographic data.

1.2 Introduction to Azulene

1.2a *The Dipole Moment of Azulene & Its Potential for Use in Molecular Electronics*

Azulene, a naturally occurring aromatic hydrocarbon with a molecular formula of $C_{10}H_8$, exhibits an array of unique physicochemical properties that make it an attractive platform for materials research. Azulene consists of fused five- and seven-membered carbon rings, and, as will be discussed in this section, this asymmetric structure is what gives rise to its host of distinctive

physical and chemical properties. Useful comparisons can be made between azulene and its benzenoid isomer, naphthalene, to emphasize precisely how the distinct structures of the two isomers cause notable differences in their respective properties.

To begin with, unsubstituted azulene, as shown in **Figure 1.2a**, has a molecular dipole of 1.08 Debye.[7]

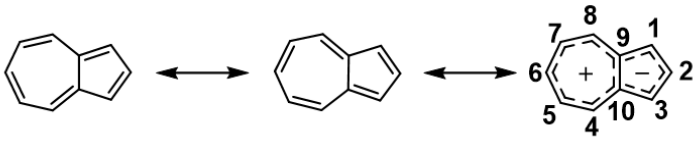

Figure 1.2a: Resonance forms and carbon labeling scheme of azulene.

The magnitude of the dipole moment is unusually high for an unsubstituted aromatic hydrocarbon, and it arises due to an intramolecular charge transfer from the seven-membered ring to the five-membered ring of azulene. Azulene's dipole moment and its conjugated π-system render it as a potential alternative to benzenoid systems in molecular electronics applications. Indeed, due to its significant dipole moment, azulene could act as a molecular rectifier or diode by conducting flow of electrons along the direction of its molecular axis.[8]

1.2b *The Frontier Molecular Orbitals of Azulene*

Azulene also displays peculiar and potentially useful electronic and photophysical properties. The frontier molecular orbitals, the Highest Occupied Molecular Orbital (HOMO) and the Lowest Unoccupied Molecular Orbital (LUMO), are complementary with respect to their orbital densities on azulene. For comparison, the frontier molecular orbitals of naphthalene, the benzenoid isomer of azulene, do not exhibit this complementary pattern. Rather, the HOMO and LUMO of naphthalene are spatially identical.[7]

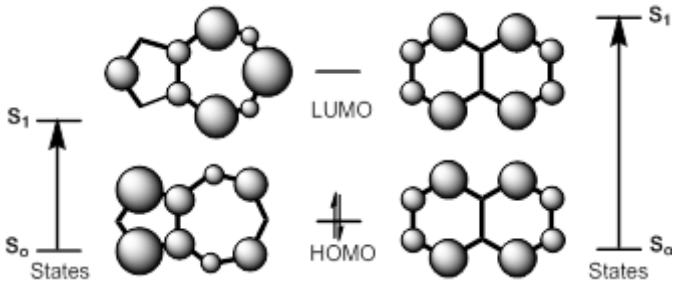

Figure 1.2b: Schematic of the frontier molecular orbitals of azulene (left) and naphthalene (right).[7]

Due to the spatially complementary nature of the HOMO and LUMO of azulene, a HOMO→LUMO excitation physically separates the electron in the excited state from the electron that remains in the ground state. This separation of electrons reduces electron-electron repulsions. In contrast, an electronic excitation in naphthalene does not reduce electrostatic repulsions since the electrons in both SOMOs are not distanced from one another after the excitation. Hence, the HOMO→LUMO transition in azulene is a lower-energy transition than that of its isomer due to the reduction of electronic repulsions in the excitation process. For this reason, azulene can absorb lower-energy radiation within the visible range, causing it to effuse an azure-blue color for which it is named. In contrast, naphthalene absorbs higher-energy ultraviolet radiation and therefore appears colorless to the human eye.

In addition to endowing azulene with its azure-blue color, the complementary frontier molecular orbitals provide chemists a mechanism with which to finely tune the HOMO-LUMO energy gap. By installing electron-withdrawing or electron-donating groups (EWG and EDG, respectively) on the odd-numbered carbons, (**Figure 1.2a**) the energy of the HOMO may be altered while leaving the LUMO unchanged. Conversely, chemistry at the even-positioned carbons modifies the LUMO but not the HOMO. Therefore, functionalization of the carbons at even positions, odd positions, or both provides for a high degree of control over the HOMO-LUMO energy gap. This feature of azulene may afford derivatives that could prove to be useful in a

number of applications, from photovoltaic devices to use as building blocks for luminescent chemosensing.

1.2c *Azulene Violates Kasha's Rule*

In addition to its significant dipole moment and complementary frontier molecular orbitals, azulene displays another intriguing property that makes it attractive for use in luminescent chemosensing, namely, azulene exhibits multiple fluorescence emissions. In fact, azulene is known to fluoresce dominantly from the second singly excited state (S_2) and less intensely from the S_1 state. This dominant S_2 emission is not only unusual, but actually violates Kasha's Rule for photoluminescent emission, which maintains that emission only occurs from the lowest-energy excited state.[7] Azulene does not obey Kasha's Rule due to the large energy separation between the S_1 and S_2 states. This gap between S_1 and S_2 reduces Franck-Condon overlap between the lower-energy vibrational wavefunctions in the S_2 state and the higher-energy vibrational wavefunctions of the S_1 state, making internal conversion via vibrational relaxation from S_2 to S_1 less likely.[9] Thus, electrons excited past the S_1 state often relax to the lowest-energy vibrational state in S_2, and fluoresce back to S_0.

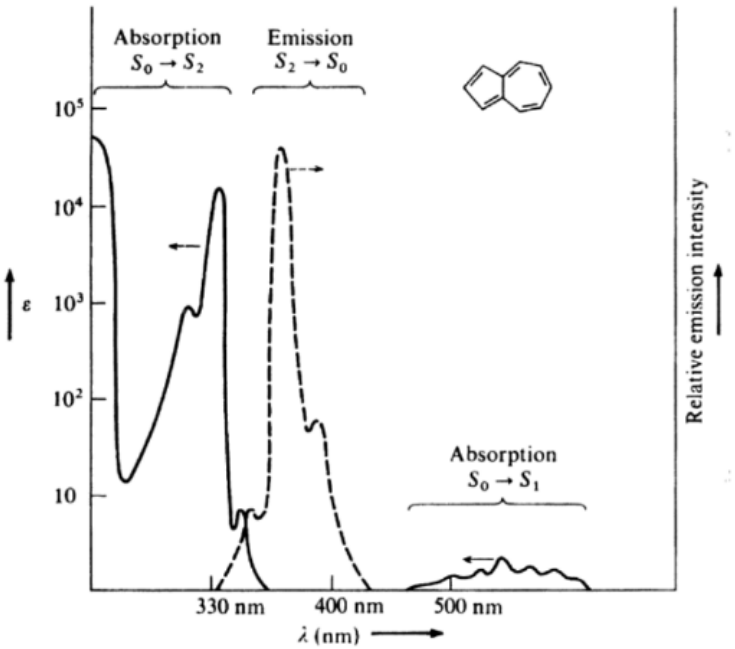

Figure 1.2c: Absorption and emission spectrum of azulene; note the dominant fluorescence from S_2.[9]

Azulenic derivatives are inherently poised for use in luminescent chemosensing due to the possibility of highly tunable frontier molecular orbitals and luminescence from multiple excited states. The forthcoming chapters discuss a family of azulenylthiolate gold(I) complexes that have been synthesized and characterized with the aim of developing materials that combine the novel and highly photoluminescent properties of both azulene and gold(I)-thiolates.

Chapter 1 References:

[1] Hakkinen, Hannu; *"The gold-sulfur interface at the nanoscale,"* Nature Chem., **2012**, 4, 443-455.

[2] Foley, J.; Fort, C.R.; McDougal, K.; Bruce, M.R.M.; Bruce, A.E.; *"Electronic and Steric Effects in Gold(I) Phosphine Thiolate Complexes,"* J. Metal Based Drugs, **1994**, 1, 405-417.

[3] Yam, W.W.V.; Chan, C.L.; Li, C.K.; Wong, K.M.C.; *"Molecular design of luminescent dinuclear gold(I) thiolate complexes; from fundamentals to chemosensing,"* Coord. Chem. Rev., **2001**, 216-217, 173-194.

[4] Kim, Y.; Pietsch, T.; Erbe, A.; Belzig, W.; Scheer, E.; "*Benzenedithiol: A Broad-Range Single-Channel Molecular Conductor,"* Nano Letters, **2011**, 11, 3734-3738.

[5] Bardajı´, M.; Calhorda, M.J.; Costa, P.J.; Jones, P.G.; Laguna, A.; Perez, M.R.; Villacampa, M.D.; *"Synthesis, Structural Characterization, and Theoretical Studies of Gold(I) and Gold(I) Gold(III) Thiolate Complexes: Quenching of Gold(I) Thiolate Luminescence,"* J. Inorg. Chem., **2006**, 45, 1059-1068.

[6] Schmidbaur, Hubert; *"The Aurophilicity Phenomenon: A Decade of Experimental Findings, Theoretical Concepts and Emerging Applications,"* Gold Bulletin, **2000**, 33, 3-10.

[7] Shevyakov, S. V.; Li, H.; Muthyala, R.; Asato, A. E.; Croney, J. C.; Jameson, D. M.; Liu, R. S. H. *"Orbital Control of the Color and Excited State Properties of Formylated and Fluorinated Derivatives of Azulene,"* J. Phys. Chem. A **2003**, 107, 3295-3299. (b) Liu, R. S.H. *"Colorful Azulene and Its Equally Colorful Derivatives,"* J. Chem. Ed. **2002**, 79, 183-185.

[8] Scheetz, K. J.; Spaeth, A. D.; Vorushilov, A. S.; Powell, D. R.; Day, V. W.; Barybin, M. V. *"The 2,6-Dimercaptoazulene Motif: Efficient Synthesis and Completely Regioselective Metallation of its 6-Mercapto Terminus,"* Chemical Science, **2013**, 4, 4267 – 4272.

[9] Turro, N.J; *"Modern Molecular Photochemistry,"* University Science Books, **1991**, 147-149.

Chapter 2:

Introduction to & Synthesis of Mercaptoazulene Variants & Their Complexes with Gold(I)

2.1 Introduction to the Chemistry of Mercaptoazulenes

2.1a *Chemistry of Mercaptoazulenes Along the Azulenic Molecular Axis*

Inspired by a series of theoretical papers that suggested the linear 2,6-substituted azulene motif could exhibit charge-transport capabilities, Barybin et al. developed syntheses for a mosaic of azulenylthiolate gold(I) complexes with hopes of assessing their potential for use in molecular electronics.[1] All of the complexes of interest feature thiolate junctions to gold(I) at the 2 and/or 6 positions on azulene in order to exploit the molecular dipole in charge transfer applications. However, in addition to their potential use in molecular electronics, these mercaptoazulene ligands and their complexes with gold(I) represented unexplored yet inherently intriguing systems for optical sensing/luminescent chemosensing as they may possess the desirable photophysical properties discussed in Chapter 1.

Figure 2.1a enumerates the specific azulenylthiolate gold(I) complexes that have been synthesized thus far by members of the Barybin Group.[1-3]

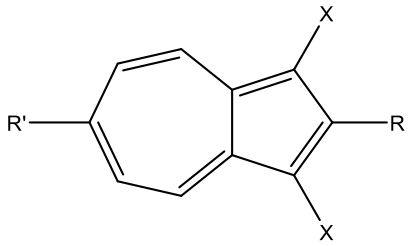

(2.2a) R = SH, R' = H, X = CO_2Et
(2.2b) R = SH, R' = azulenyl, X = CO_2Et
(2.2c) R = SH, R' = H, X = H
(2.2d) R = SH, R' = SH, X = CO_2Et
(2.2e) R = H, R' = SH, X = CO_2Et
(2.3b) R = S(PPh_3)AuCl, R' = H, X = H
(2.3c) R = S(PPh_3)AuCl, R' = H, X = CO_2Et
(2.3d) R = H, R' = S(PPh_3)AuCl, X = CO_2Et
(2.3e) R = S(PPh_3)AuCl, R' = azulenyl, X = CO_2Et
(2.3f) R = SH, R' = S(PPh_3)AuCl, X = CO_2Et
(2.3g) R = S(PPh_3)AuCl, R' = S(PPh_3)AuCl, X = CO_2Et

Figure 2.1a: The family of azulenylthiolate gold(I) complexes synthesized by Barybin et al.[1,2]

2.1b *Acid-Base Reactions of Azulenylthiolate Gold(I) Complexes*

Once synthesized, the characterization of the physical and chemical properties of these gold(I) complexes was undertaken, of which some of the results are discussed in this thesis for the first time. A preliminary reactivity study performed on these complexes qualitatively determined the series of the relative acidities of the thiol on the respective mercaptoazulene ligands. The results of this qualitative reactivity study are highlighted in **Figure 2.1b**, as several mercaptoazulenes are shown in order of increasing pK_a.[2]

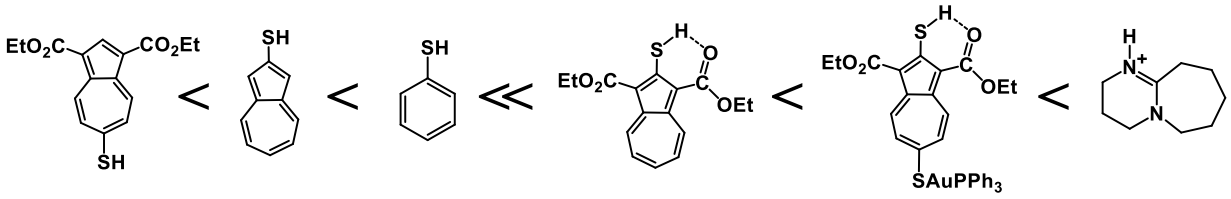

Figure 2.1b: Qualitative series of thiol pK_a values for several mercaptoazulene species. For reference, the pK_a of thiophenol is 10.28.[4,5]

One significant finding from this reactivity study was the notable difference in the acidities of the thiol groups on the 2-mercapto- and 6-mercapto- ethoxycarbonylazulene isomers. The markedly less-acidic nature of the former has been attributed to the formation of a hydrogen bond between the carbonyl oxygen of one of the ethoxycarbonyl substituents and the thiol hydrogen. This favorable interaction decreases the acidity of the thiol, a phenomenon which does not occur for its 6-thiol isomer due to its inability to form any such hydrogen bond.[1,6] This hydrogen bonding motif is well illustrated in the X-ray crystal structure depicted in **Figure 2.1c.**[6]

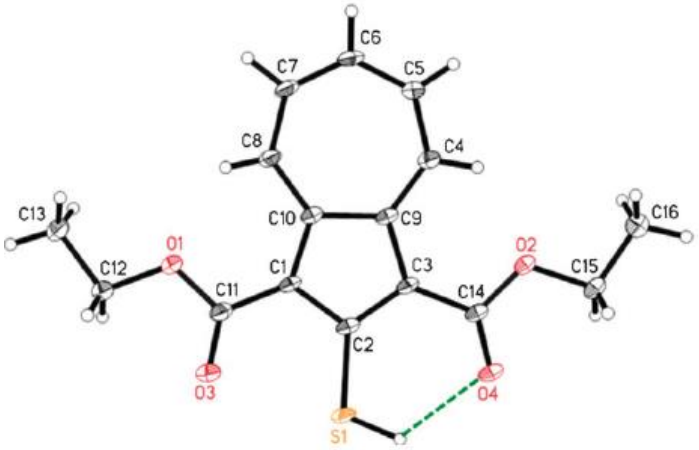

Figure 2.1c: Molecular structure of species 2-mercapto-1,3-diethoxycarbonylazulene with 50% thermal ellipsoids. Note the intramolecular S-H···O hydrogen bond.[5]

This hydrogen bonding between capability of the carbonyl oxygen affects the stability in solution of the corresponding gold(I) complex of this ligand, which will be discussed in more detail shortly. The remainder of this chapter will discuss the specific synthetic procedures employed to generate several mercaptoazulene species and their complexes with gold(I), as well as elaborations on findings related to the above acid-base reactivity studies.

2.2 Synthesis of Several Mercaptoazulene Ligands

2.2a *2-mercapto-1,3-diethoxycarbonylazulene*

2-chloro-1,3-diethoxycarbonylazulene (0.400 g, 1.3 mmol) and sodium hydrosulfide (3.795 g, 45.5 mmol) were placed in a 150 mL round bottom flask. 40 mL of 65% aqueous ethanol solution were then placed in the flask. The solution was then left to reflux and stir for two hours. After two hours, the heat was turned off and 110 mL of water was added. The solution was then stirred for ca. 20 hours. Then, the solution was subject to extraction with pentane (3 x 100 mL) in a separation funnel. The aqueous layer was then acidified with H_2SO_4 (3 M), causing 2-mercapto-1,3-diethoxycarbonylazulene to precipitate out of solution. To collect the product, the aqueous

layer and precipitate were then extracted with dichloromethane (3 x 100 mL). The extract was then dried over anhydrous sodium sulfate and passed through a short silica column using CH_2Cl_2 as eluent. All solvents removed via rotary evaporation, leaving behind small, orange, needle-like crystals of product in a 42.7% yield (0.1703 g, 0.556 mmol).

2.2b *Alternative synthesis of 2-mercapto-1,3-diethoxycarbonylazulene*

2-chloro-1,3-diethoxycarbonylazulene (0.715 g, 2.32 mmol), 35 mL of pyridine, and methyl 3-mercaptopropionate (0.946 g, = 0.872 mL, 3.07 mmol) were placed in a 500 mL round bottom flask. The solution was stirred at 90º C for one hour. The solution was the extracted with dichloromethane and water, and the organic layer was then washed with water and 3 M H_2SO_4. The organic extracts were then dried over anhydrous sodium sulfate. The product was dried down to a dark red oil, and purified on a silica column with benzene and ethyl acetate as eluent. The product was then dried under reduced pressure, leaving behind a dark red oil. The red oil was placed in a round bottom flask with 50 mL of 100 % ethanol. 0.336 g of NaOH were dissolved in the ethanol and the solution was left to stir for two hours. Then, the solution was diluted with 200 mL of water and neutralized with 3 M HCl, yielding a precipitate. The precipitate was filtered using a ceramic frit filter and was washed with water. Then, the precipitate was extracted with dichloromethane and water (3 x 200 mL water). The water was removed with anhydrous sodium sulfate. The product was then dissolved in CH_2Cl_2 and subject to normal phase column chromatography using dichloromethane as eluent. The product was recrystallized in dichloromethane which was then layered with pentane, yielding orange crystals of 2-mercapto-1,3-diethoxycarbonylazulene in a 42% yield(0.300 g, 0.97 mmol). ^{1}H NMR and ^{13}C NMR characteristics of the product were identical to those of the bona fide 2-mercapto-1,3-diethoxycarbonylazulene. ^{1}H NMR (400 MHz, $CDCl_3$, 25 °C): δ 1.50 (t, $^3J_{HH}$ = 8 Hz, 6H, C*H*$_3$),

4.49 (q, $^{3}J_{HH}$ = 8 Hz, 4H, C*H*$_2$), 7.58 (t, $^{3}J_{HH}$ = 10 Hz and 12 Hz, 2H, $H^{5,7}$), 7.69 (t, $^{3}J_{HH}$ = 12 Hz, 1H, H^{6}), 7.71 (s, 1H, S*H*) 9.34 (dd, $^{3}J_{HH}$ = 10 Hz and 12Hz, 2H, $H^{4,8}$) ppm. ^{13}C NMR (100.6 MHz, $CDCl_3$, 25 °C): δ 14.5 (*C*H$_3$), 60.7 (*C*H$_2$), 113.7, 131.7, 135.5, 138.0, 143.9, 155.7, 166.0 (*C*O$_2$Et) ppm.[6]

2.2c *Synthesis of 2-mercaptoazulene*

H_3PO_4 (5.399 g, 55 mmol) was placed into a 100 mL flask with 2-mercapto-1,3-diethoxycarbonylazulene (0.1676g, 0.55 mmol). The round bottom flask was placed in an oil bath at 115º C for one hour. Then, the temperature was raised to 130º C for an additional hour. The solution was then transferred to a separation funnel and quenched with 200 mL of water, which formed a purple precipitate. The product was extracted with benzene (2 x 30 mL) and dried over anhydrous sodium sulfate. All solvents were removed via rotary evaporation, producing a lavender powder of 2-mercaptoazulene in an 87.3% yield (0.077 g, 0.48 mmol). ^{1}H NMR (400 MHz, $CDCl_3$, 25 °C): δ 3.88 (s, 1H, S*H*), 7.12 (s, 2H, $H^{1,3}$), 7.14 (dd, $^{3}J_{HH}$ = 12 Hz and 10 Hz, 2H, $H^{5,7}$), 7.44 (t, J = 10 Hz, 1H, H^{6}), 8.04 (d, $^{3}J_{HH}$ = 12 Hz, , 2H, $H^{4,8}$) ppm. ^{13}C NMR (100.6 MHz, $CDCl_3$, 25 °C): δ 116.6, 124.5, 133.0, 135.4, 140.7, 140.8 ppm. [6]

2.3 Synthesis of Gold(I) Complexes with Azulenylthiolate Adducts

The following procedures were carried out using standard Schlenk techniques under an inert atmosphere of argon. All solvents used in reactions were distilled and stored under argon. All stirring processes were performed with flasks protected from ambient lighting. Recrystallizations were performed for 24 hours or less to avoid degradation of the metal complexes.

2.3a *Synthesis of triphenylphosphine gold(I) chloride*

Triphenylphosphine (0.0178 g, 0.06789 mmol) was placed into a 100 mL side-arm round bottom flask (SARB). The flask was cycled three times under an inert atmosphere of argon. Then, chloro(dimethylsulfide)gold(I) (0.0205 g, 0.06955 mmol) was transferred under an inert atmosphere into the flask. 20 mL of CH_2Cl_2 stored under argon were cannulated into the flask and stirred for one hour. Next, the dichloromethane was removed via vacuum, leaving behind a brown residue of triphenylphosphine gold(I) chloride which carried forward immediately in the syntheses of **2.3b, 2.3c, 2.3d, 2.3e, 2.3f** or **2.3g**.

2.3b *Synthesis of 2-thiolate-azulene gold(I)-triphephenylphosphine*

Triphenylphosphine gold(I) chloride (0.146 g, 0.296 mmol), sodium hydroxide (0.075 g, 1.869 mmol) and 2-mercaptoazulene (0.050 g, .312 mmol) were placed in a 250 mL SARB. Then, ca. 20 mL of methanol were added to the SARB and the solution was stirred for one. 20 mL of CH_2Cl_2 were then added to the solution via cannula and stirred for 24 hours. All solvents were removed under vacuum using an external trap connected to a Schlenk line. The SARB was refilled with argon and transferred to a glove box. The brown contents of the SARB were dissolved in CH_2Cl_2 and filtered through celite in a small Pasteur pipette. The filtrate was collected and recrystallized in distilled CH_2Cl_2 layered with distilled pentane at -20^o C. The recrystallization yielded relatively long, brown crystals that showed slight impurities by ^{1}H NMR. To remove any remaining 2-mercaptoazulene from the product, the crystals were extracted in a separation funnel with 10 mL of CH_2Cl_2, 5 mL H_2O and 2-3 mL of triethylamine. The CH_2Cl_2 extract was then subject to a short alumina column to remove any unreacted triphenylphosphine gold(I) chloride.

The excess triphenylphosphine gold(I) chloride came off the column first in a yellow band, followed by the dark brown band of the desired product. 2-thiolate-azulene gold(I)-triphephenylphosphine was isolated in a 27.9% yield as a black-cherry colored crystalline solid after all solvents were removed via rotary evaporation. (0.0537 g, 0.087 mmol) ^{1}H NMR (400 MHz, $CDCl_3$, 25 ^{o}C) δ 7.86 (d, $^{3}J_{HH}$ = 9.6 Hz, 2H, *H* ^{4,8}), 7.63 – 7.47 (m, 15 H, PPh_3), 7.33 (s, 2H, *H* ^{1,3}), 7.27 (t, $^{3}J_{HH}$ = 9.8 Hz, 1H, *H* ^{6}), 7.05 (t, $^{3}J_{HH}$ = 9.7 Hz, 2H, *H* ^{5,7}) ppm. ^{13}C{^{1}H} NMR (126 MHz, $CDCl_3$, 25 ^{o}C) δ 155.19, 140.79, 134.44, 134.33, 132.86, 131.90, 131.88, 130.27, 129.43, 129.34, 123.80, 121.16 (azulenic *C* and PPh_3) ppm. ^{31}P{^{1}H} NMR (162 MHz, $CDCl_3$, 25 °C): 38.34 ppm.[2]

2.3c *Synthesis of 2-thiolate-1,3-diethoxycarbonylazulene gold(I) triphenylphosphine*

Triphenylphosphine gold(I) chloride (0.155 g, 0.3135 mmol), sodium hydroxide (0.0792 g, 1.98 mmol) and 2-mercapto-1,3-diethoxycarbonylazulene (0.0994 g, 0.33 mmol) were placed in a 250 mL SARB. 20 mL of methanol were added to the SARB and the solution was stirred for one hour. Then, 30 mL of CH_2Cl_2 were added via cannula and the solution was left to stir for 24 hours. Next, the solvents were removed under vacuum with an external Schlenk trap. The resulting product was filtered with CH_2Cl_2 through celite in a Pasteur pipette. The filtrate was collected and the solvent was dried off. The minimum amount of CH_2Cl_2 required to dissolve all solids was added and layered with pentane and stored at -20^{o} C for recrystallization. Crystals were formed of 2-thiolate-1,3-diethoxycarbonylazulene gold(I) triphenylphosphine and were isolated in a 62.8% yield (0.162 g, 0.207 mmol). ^{1}H NMR (400 MHz, CD_2Cl_2, 25 ^{o}C) δ 8.69 (d, $^{3}J_{HH}$ = 10.0 Hz, 2H, H ^{4,8}), 7.60 – 7.41 (m, 18H, PPh_3 + H ^{5,6,7}), 4.22 (q, $^{3}J_{HH}$ = 7.1 Hz, 4H, -CH_2-), 1.31 (t, $^{3}J_{HH}$ = 7.1 Hz, 6H, -CH_3) ppm. ^{13}C{ ^{1}H} NMR (126 MHz, CD_2Cl_2, 25 ^{o}C) δ 167.09 (-CO_2-), 159.90, 141.69,

136.38, 134.79, 133.00, 132.25, 129.77, 129.67, 129. 60, 122.06 (azulenic C and PPh_3), 60.88 (-CH_2-), 14.81 (-CH_3). $^{31}P\{^1H\}$ NMR (162 MHz, $CDCl_3$, 25 °C): 36.49 ppm. [2]

2.3d *Synthesis of 6-thiolate-1,3-diethoxycarbonylazulene gold(I) triphenylphosphine*

Triphenylphosphine gold(I) chloride (0.081 g, 0.165 mmol), sodium hydroxide (0.0469 g, 1.17 mmol) and 6-mercapto-1,3-diethoxycarbonylazulene (0.0532 g, 0.165 mmol) were placed in a 250 mL SARB. 20 mL of methanol were added to the SARB via cannula and the solution was stirred for 30 minutes. Then, 30 mL CH_2Cl_2 were cannulated into the SARB and the solution was stirred for ca. 20 hours. The solvents were removed under vacuum and the product left behind was filtered through celite in a Pasteur pipette with CH_2Cl_2. The filtrate was collected and all solvent was dried off. Then, the minimum amount of CH_2Cl_2 required to dissolve all solids was added and layered with pentane. This solution was left to recrystallize at -20º C. 6-thiolate-1,3-diethoxycarbonylazulene gold(I) triphenylphosphine was obtained in red crystalline form at 72% yield (0.924 g, 0.119 mmol). ^1H NMR (400 MHz, $CDCl_3$, 25 ºC) δ 9.20 (d, $^3J_{HH}$ = 11.3 Hz, 2H, H ^{4,8}), 8.48 (s, 1H, H ^{2}), 8.26 (d, $^3J_{HH}$ = 11.3 Hz, 2H, H ^{5,7}), 7.60 – 7.48 (m, 15H, PPh_3), 4.38 (q, $^3J_{HH}$ = 7.1 Hz, 4H, -CH_2-), 1.42 (t, $^3J_{HH}$ = 7.1 Hz, 6H, -CH_3) ppm. $^{13}C\{^1H\}$ NMR (126 MHz, $CDCl_3$, 25 ºC) δ 165.56 (-CO_2-), 140.99, 139.09, 135.30, 134.75, 134.30, 134.19, 132.18, 132.16, 129.61, 129.52, 129.10, 128.64, 115.82 (azulenic C and PPh_3) 59.76 (-CH_2-), 14.72 (-CH_3) ppm. $^{31}P\{^1H\}$ NMR (162 MHz, $CDCl_3$, 25 °C): 37.98 ppm. FTIR (CH_2Cl_2): ν_{CO} 1685 s cm^{-1}. [2]

2.3e *Synthesis of 2-thiolate-1,3-diethoxycarbonyl-2',6-biazulene gold(I) triphenylphosphine*

Triphenylphosphine gold(I) chloride (0.120 g, 0.2432 mmol), sodium hydroxide (0.0612 g, 1.53 mmol) and 2-mercapto-1,3-diethoxycarbonyl-2',6-biazulene (0.1104 g, 0.256 mmol) were placed in a 100 mL SARB. 10 mL of methanol was added to the SARB and the solution was left

to stir for one hour. Then, 15 mL of CH_2Cl_2 were added and the solution was stirred for 24 hours. All solvents were removed under vacuum with an external Schlenk trap. The product was run through a celilte filter in a Pasteur pipette and all solvent was dried off from the filtrate. Then, the minimum amount of CH_2Cl_2 required to dissolve all solids was added to the product and layered with pentane. This solution was left to recrystallize at -20º C. The mother liquor was decanted, yielding product with an olive-green color and metallic sheen in 79.6% yield. (0.1741 g, 0.204 mmol). ^{1}H NMR (500 MHz, $CDCl_3$, 25.2ºC) δ 8.84 (d, $^3J_{HH}$ = 11.4 Hz, 2H, *H* ^{4,8}), 8.24 (d, $^3J_{HH}$ = 9.2 Hz, 2H, *H* $^{4',8'}$), 8.09 (d, $^3J_{HH}$ = 11.2 Hz, 2H, *H* ^{5,7}), 7.66 (s, 2H, *H* $^{1',3'}$), 7.56 – 7.41 (m, 16 H, *H* 6' + PPh_3), 7.11 (t, $^3J_{HH}$ = 9.8 Hz, 2H, *H* $^{5',7'}$), 4.30 (q, $^3J_{HH}$ = 7.1 Hz, 4H, -C*H*$_2$-), 1.37 (t, $^3J_{HH}$ = 7.1 Hz, 6H, -C*H*$_3$) ppm. ^{13}C{^{1}H} NMR (126 MHz, $CDCl_3$, 25.2ºC) δ 166.77 (-*C*O_2-), 160.14, 151.59, 143.70, 141.31, 140.88, 137.67, 137.21, 134.28, 134.17, 131.82, 131.68, 131.66, 129.61, 129.46, 129.21, 129.16, 129.12, 124.29, 121.71, 115.94 (azulenic *C* and PPh_3), 60.31 (-*C*H_2-), 14.60 (-*C*H_3) ppm. ^{31}P{^{1}H} NMR (162 MHz, $CDCl_3$, 20.8°C): 36.41 ppm. [2]

2.3f *Synthesis of 2-mercapto-6-thiolate-1,3-diethoxycarbonylazulene gold(I) triphenylphosphine*

Triphenylphosphine gold(I) chloride (0.051 g, 0.104 mmol), triethylamine (0.0102 g = 0.014 mL, 0.104 mmol) and 2,6-mercapto-1,3-diethoxycarbonylazulene (0.0347 g, 0.104 mmol) were placed in a 150 mL SARB. 10 mL of THF were added via cannula to the SARB and the solution was stirred for five hours. The solution was then concentrated under vacuum leaving ~2 mL solvent behind. 5 mL of pentane were added to the solution to cause the red-orange product to precipitate out of solution. The product was then filtered and recrystallized in dichloromethane layered with pentane at -20ºC. Small, red-orange crystals of 6-thiolate-2-mercapto-1,3-diethoxycarbonylazulene gold(I) triphenylphosphine were obtained 47.6% yield (0.040g, 0.0495

mmol). ^{1}H NMR ($CDCl_3$, 400 MHz, 25 °C): δ 1.48 (t, $^{3}J_{HH}$ = 8 Hz, 6H, C*H*$_3$), 4.47 (q, $^{3}J_{HH}$ = 8 Hz, 4H, C*H*$_2$), 7.49 (s, 1H, S*H*) 7.55 (m, 15 *H*, PPh_3), 8.20 (d, $^{3}J_{HH}$ = 12 Hz, 2H, *H*^{5,7}), 8.97 (d, $^{3}J_{HH}$ = 12 Hz, 2H, *H*^{4,8}) ppm. ^{13}C{^{1}H} NMR ($CDCl_3$, 126 MHz, 25 °C): δ 14.5 (*C*H_3), 60.2 (*C*H_2), 113.2, 128.6, 129.0, 129.4 (d, $^{2}J_{CP}$ = 11.3 Hz), 132.0 (d, $^{3}J_{CP}$ = 2.5 Hz), 132.4, 134.1 (d, $^{1}J_{CP}$ = 13.8 Hz), 135.6, 141.1, 149.9, 165.3 (CO_2*Et*), 166.2 (*C*O_2Et) ppm. ^{31}P{^{1}H} NMR (162 MHz, $CDCl_3$, 25 °C): 37.54 ppm. ^{31}P{^{1}H} NMR (202 MHz, CD_2Cl_2, 25 °C): 37.89 ppm. UV-Vis (CH_2Cl_2, λ_{max} (ε×10^{-3} M-1 cm^{-1}), 24 °C): 235 (35.4), 245 (32.8), 275 (26.2), ~295 (15.1) sh, 325 (21.0), 365 (41.6), ~425 (25.2) sh, 445 (39.1) nm.[1]

2.3g *Synthesis of 2,6-dithiolate-1,3-diethoxycarbonyl azulene gold(I) triphenylphosphine*

Triphenylphosphine gold(I) chloride (0.0233 g, 0.0471 mmol), sodium hydroxide (0.0155 g, 0.297 mmol), and **2.3f** (0.0401 g, 0.0495 mmol) were placed into a 150 mL SARB. 10 mL of methanol were added and the solution was stirred for 30 minutes. Then, 10 mL of dichloromethane were added and the solution was left to stir for 24 hours. All volatiles were then removed under vacuum, leaving a brown-red solid behind. The solid was then dissolved in dichloromethane and filtered through a short plug of alumina. Then, the filtrate was concentrated to a minimum quantity of dichloromethane and was layered with pentane for recrystallization at -20 º C, yielding reddish-brown crystals in 43.4% yield (0.0269 g, 0.021 mmol). ^{1}H NMR ($CDCl_3$, 400 MHz, 20 °C): δ 1.32 (t, $^{3}J_{HH}$ = 7 Hz, 6H, C*H*$_3$), 4.23 (q, $^{3}J_{HH}$ = 7 Hz, 4H, C*H*$_2$), 7.53 (m, 30 *H*, PPh_3) 8.01 (d, $^{3}J_{HH}$ = 11.0 Hz, 2H, *H*^{5,7}) 8.42 (d, $^{3}J_{HH}$ = 11.0 Hz, 2H, *H*^{4,8}) ppm. ^{31}P{^{1}H} NMR (202 MHz, CD_2Cl_2, 22 °C): 37.19 (broad singlet) ppm. ^{31}P NMR (202 MHz, CD_2Cl_2, -40 °C): 37.95, 36.19 ppm. UV-Vis (CH_2Cl_2, λ_{max} (ε×10^{-3} M^{-1} cm^{-1}), 24 °C): 290 (17.0), ~320 (24.0) sh, ~340 (32.2), 365 (40.3), ~450 (28.9) sh, 475 (38.8) nm.[1]

2.4 Findings From the Optimization of the Synthesis 2-Azulenylthiolate Gold(I) Triphenylphosphine

2.4a *Importance of Purity of 2-Mercaptoazulene Precursor*

Synthesizing and isolating the 2-thiolate-azulene gold(I) triphephenylphosphine complex proved quite difficult due to the complex's unprecedented instability in solution. However, after a number of failures, the procedure detailed in **2.3b** represents a synthetic pathway to the desired complex that ensures purity and bypasses purification methods that might jeopardize the stability of the final product. The trial and error process of synthetic optimization, synthetic pitfalls, and the unexpected insights into the reactivity of these gold complexes are discussed herein.

The first principal concern in this synthesis was the purity of the 2-mercaptoazulene ligand. **2.3c** describes the de-esterification of 2-mercapto-1,3-diethoxycarbonylazulene via acidification with phosphoric acid to produce 2-mercaptoazulene. This process is highly sensitive to temperature; even minute fluctuations in the temperature over the two-hour heating process may yield mixed products containing mercaptoazulenes with one, two or no ethoxycarbonyl groups. These products are difficult to separate, and the aggressive highly acid, high-temperature conditions of the reaction can degrade the products if left to react for time significantly longer than two hours. Thus, it was crucial to control the reaction conditions with great care throughout the course of the reaction to produce pure 2-mercaptoazulene.

2.4b *Insights into the Acid-Base Chemistry of the 2-Azulenyltiholate Congeners from the Purification of 2-Azulenylthiolate Gold(I) Triphenylphosphine*

Purifying 2-azulenylthiolate gold(I) triphenylphosphine required more sensitive techniques than did purification of any of the other complexes in this work. None of the azulenylthiolate gold(I) complexes are stable upon subjection to silica column chromatography, as silica's acidic nature cleaves the Au-S bond and can lead to formation of disulfide linkages between azulenylthiolate ligands or regeneration of the protonated thiol groups. Therefore, recrystallization in dichloromethane layered with pentane represented a more gentle form of purification. This technique worked well for purifying the complexes featuring azulenic ligands with ethoxycarbonyl substituents, and was implemented in several trials for the purification of 2-azulenylthiolate gold(I) triphenylphosphine, producing mixed results. However, when attempted in replicate, this process often led to the degradation of the complex, as seen in the following series of ^{1}H NMR spectra.

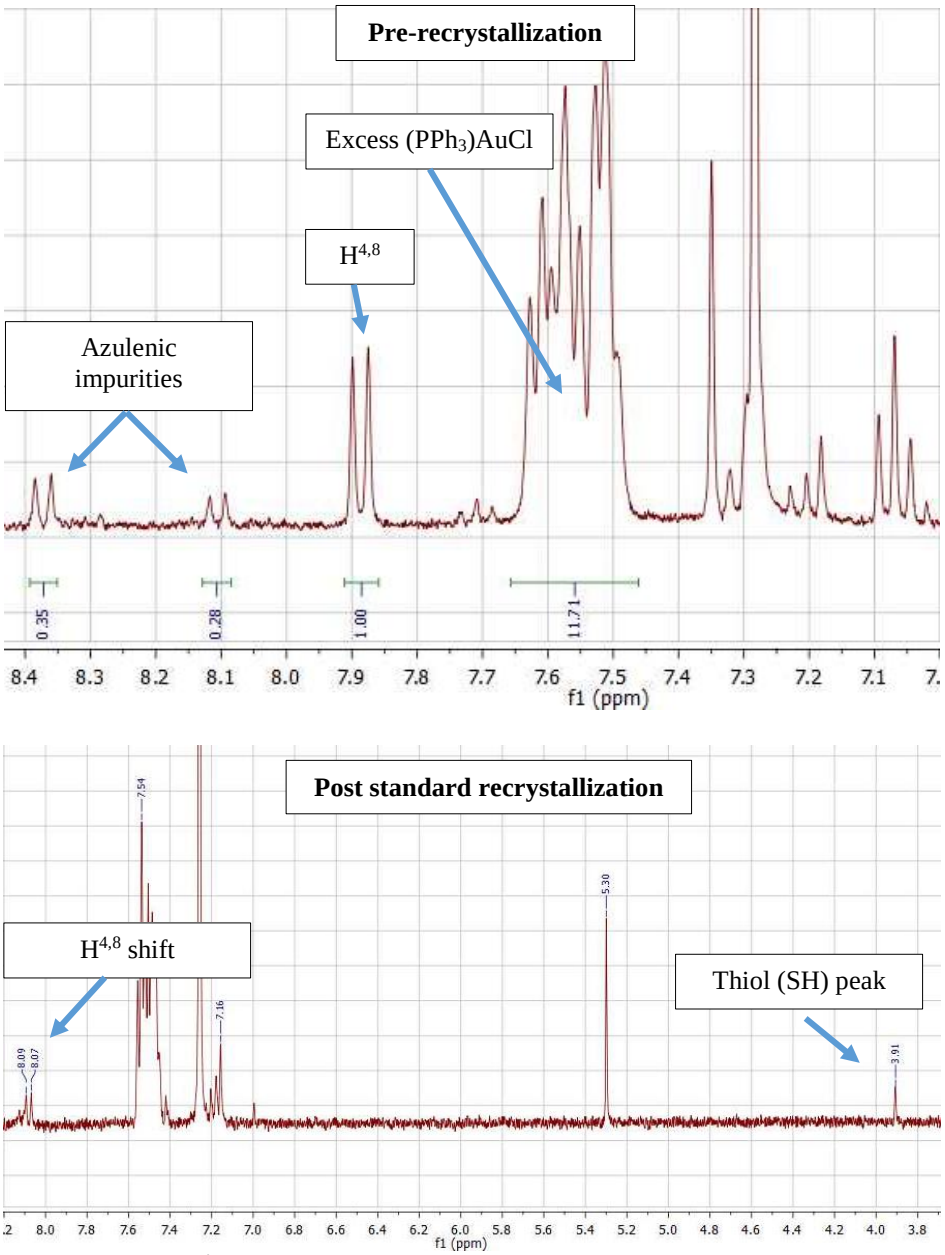

Figure 2.4b: Series of ^{1}H NMR spectra of 2-azulenylthiolate gold(I) triphenylphosphine indicating regeneration of mercaptoazulene precursor after standard recrystallization in dichloromethane and pentane.

The spectra in **Figure 2.4b** indicate the re-formation of 2-mercaptoazulene from the gold(I) complex, as demonstrated by the appearance of the thiol singlet with a chemical shift of 3.91 ppm. Additionally, the doublet associated with the 4- and 8- position carbons on azulene shifts upon

protonation to form a doublet that matches the chemical shift for these positions in the ^{1}H NMR of the 2-mercaptoazulene ligand.

The apparent cleavage and subsequent protonation of the thiolate group is attributed to the presence of minute amounts of hydrochloric acid in un-distilled CH_2Cl_2, which is formed by the hydrolysis of CH_2Cl_2 by trace amounts of water present in the solvent. Although it was known that small quantities of HCl may be present in the CH_2Cl_2 used for standard recrystallizations, it had never presented a problem in prior purifications of other azulenylthiolate gold(I) complexes. Thus the regeneration of 2-mercaptoazulene was an unexpected result. This finding was particularly peculiar in light of the fact that the congener of 2-azulenylthiolate containing ethoxycarbonyl substituents at the 1 and 3 positions was not protonated under the same conditions, despite having a thiolate with a weaker conjugate acid. This behavior indicated that the aforementioned qualitative pK_a bracketing of **Figure 2.1b** was not as simple as it initially appeared.

To explain this phenomenon, several contributing factors must be taken into consideration. Firstly, it has been established that the apparent basicity of the 2-thiolate-1,3-diethoxycarbonylazulene arises from the hydrogen bonding interaction between the carbonyl oxygen and the thiol hydrogen, effectively "embracing" the hydrogen and making deprotonation more difficult.[1] However, neglecting the hydrogen bonding interaction, one would assume that the 2-azulenylthiolate ligand would be more basic than 2-thiolate-1,3-diethoxycarbonylazulene as the latter should experience significant withdrawal of thiolate electron density due to the inductive effects of the ester oxygens. Perhaps the presence of the electron-withdrawing carbonyl oxygen on 2-thiolate-1,3-diethoxycarbonylazulene inhibits the protonation of the thiolate in the gold(I) complex by reducing the electron-accepting ability of the thiolate. However, if the thiolate is protonated, the hydrogen bonding interaction with the acidic hydrogen and carbonyl oxygen

stabilizes the protonated form. This would mean that 2-mercapto-1,3-diethoxycarbonylazulene is less acidic than 2-mercaptoazulene, but by virtue of the hydrogen bond, not the basicity of the sulfur. Therefore, in the absence of the ethoxycarbonyl substituents, the 2-azulenylthiolate sulfur should be more electron dense because it has no nearby electron-withdrawing groups to prevent the protonation of the thiolate and should act as a stronger base. Hence, protonation should be more favorable for this species than its congener, explaining why protonation of the gold(I) complex was observed during recrystallization only for the 2-azulenylthiolate complex.

Chapter 2 References:

[1] Scheetz, K. J.; Spaeth, A. D.; Vorushilov, A. S.; Powell, D. R.; Day, V. W.; Barybin, M. V. *"The 2,6-Dimercaptoazulene Motif: Efficient Synthesis and Completely Regioselective Metallation of its 6-Mercapto Terminus,"* Chemical Science, **2013**, 4, 4267 – 4272.

[2] Spaeth, A.D.; *"A Synergistic Synthetic, Spectroscopic and Computational Approach to the Design of Organometallic Platforms Featuring Linearly Functionalized Azulenic and Biazulenic Motifs,"* University of Kansas, **2014**, 1-42.

[3] Applegate, J.C.; Okeowo, M.K.; Erickson, R.A.; Neal, B.M.; Berrie, C.L.; Gerasimchuk, N.N. Barybin, M.V.; *"First π-linker featuring mercapto and isocyano anchoring groups within the same molecule: synthesis, heterobimetallic complexation and self-assembly on Au(111),"* Chem. Sci., **2016**, 7, 1422-1429.

[4] Cox, B. G.; *"Acids and Bases: Solvent Effects on Acid-base Strength,"* 1st ed. Oxford, UK: Oxford UP, **2013**.

[5] Kaupmees, K.; Trummal, A.; Leito, I.; *"Basicities of Strong Bases in Water: A Computational Study,"* Croat. Chem., **2014**, 87: 385–395.

[6] Neal, B. M.; Vorushilov, A. S.; DeLaRosa, A. M.; Robinson, R. E.; Berrie, C. L.; Barybin, M. V.; *"Ancillary Nitrile Substituents as Convenient IR Spectroscopic Reporters for Self-Assembly of Mercapto- and Isocyanoazulenes on Au(111),"* Chemical Communications, **2011**, 47, 10803-10805.

Chapter 3:

Electronic Absorption & Photoluminescence Profiles of Azulenylthiolate Gold(I) Complexes

3.1 Photoluminescence Studies of Azulenylthiolate Gold(I) Complexes

3.1a *Sources of Interference in Luminescence Spectroscopy & How to Avoid Them*

As introduced in Chapter 1, these azulenylthiolate gold(I) systems should display very unique photoluminescence profiles as they may exhibit a number of different possible charge transfer relaxation pathways, including the possibility of multiple emissions and LCMMT through aurophilic interactions. The results of several preliminary photoluminescence studies of these complexes are presented in this chapter.

The photoluminescent profiles of a number of the gold(I) complexes discussed in Chapter 2 were studied via fluorescence and phosphorescence spectroscopy. Troubles obtaining satisfactory luminescence spectra were experienced at the onset of the study, as fluorescence and phosphorescence spectra can be complicated by the prevalence of numerous sources of spectral interference. These several sources of interference, from solvent stabilizers, to second-order diffraction, to Raman scattering, made interpretation of spectra increasingly difficult as the interference was not always expected and was often initially mistaken as a signal from the analyte in question. Although not directly related to the characterization of azulenylthiolate gold(I) complexes, the following portion of this chapter is crucial in that it reveals the pitfalls of fluorescence and phosphorescence spectroscopy, and methods to circumvent them. Without having identified these sources of interference, acquisition of the desired luminescence spectra of the gold(I) complexes would not have been achieved.

The first major source of interference that was discovered arose from solvent stabilizers. All low-temperature photoluminescence scans were performed in 2-methyltetrahydrofuran for its ability to form a translucent glass in the solid state. However, 2-methyl THF photolyzes after

prolonged exposure to light, forming radicals. To prevent radical formation, most commercial 2-methyltetrahydrofuran contains trace amount of butylated hydroxytoluene (BHT) stabilizer. This stabilizer is highly luminescent, and can obscure signals from the analyte in a sample spectrum. The presence of BHT in the solvent was known, so prior to luminescence studies, the 2-methyl THF solvent was distilled. However, this proved to be an inadequate method of removing the stabilizer as the phosphorescence scans of distilled 2-methyl THF still exhibited phosphorescence from BHT. An example of the intense signal from BHT is shown below in **Figure 3.1a**.

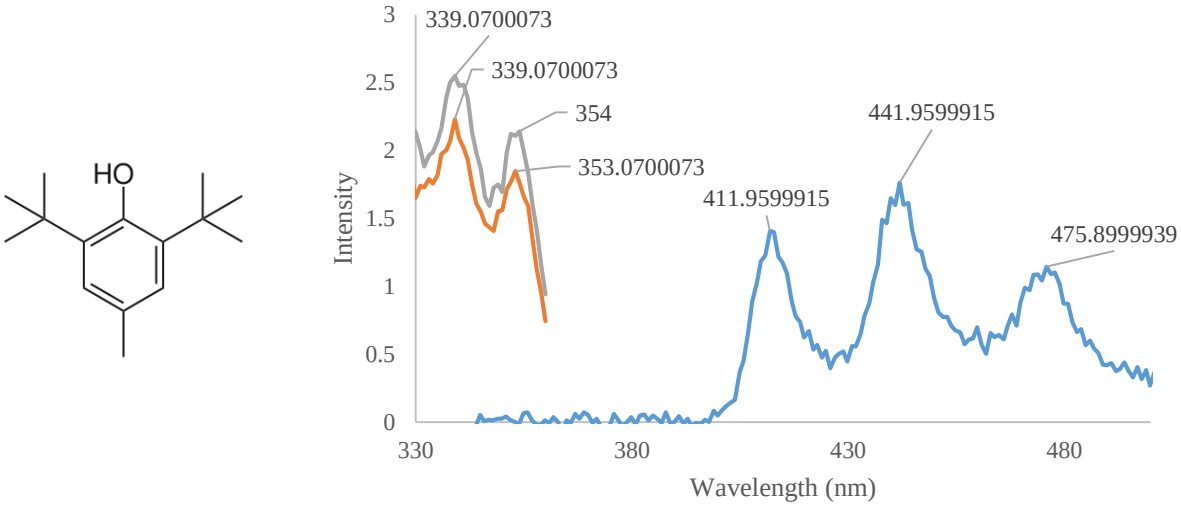

Figure 3.1a: Structure of BHT (left); phosphorescence emission spectrum of BHT (Blue); excitation spectra of BHT at 411 nm (orange); excitation scan at 441 nm (gray).

To circumvent the interference of BHT, BHT-free 2-methyl THF stored under nitrogen was purchased and implemented in subsequent photoluminescence experiments. Even upon removal of interference from BHT, interpreting photoluminescence scans remained challenging due to the presence of peaks that arise from second-order diffraction and from Raman scattering.

Second-order diffraction originates from the optical properties of light diffracted by the reflection grating used in the monochromator of a given instrument. **Figure 3.1b** shows a reflection grating that is commonly used in monochromators.[2] These types of gratings cause the dispersion

of polychromatic light upon impingement of the light on the surface of the blazed grating. The polychromatic light is partitioned into its constituent beams of light of differing wavelengths, all of which are dispersed from the grating at slightly different angles. This partitioning occurs as a result of constructive and destructive interference of light as it is dispersed from the grating. Constructive interference only occurs for beams of light that have wavelengths that are integer multiples of each other.[3] Ideally, only light of first-order diffraction should reach the detector. However, often times the first-order and second-order diffracted light beams overlap, as in demonstrated in **Figure 3.1b**. This phenomenon causes a peak at twice the first-order wavelength to appear in the emission spectrum.

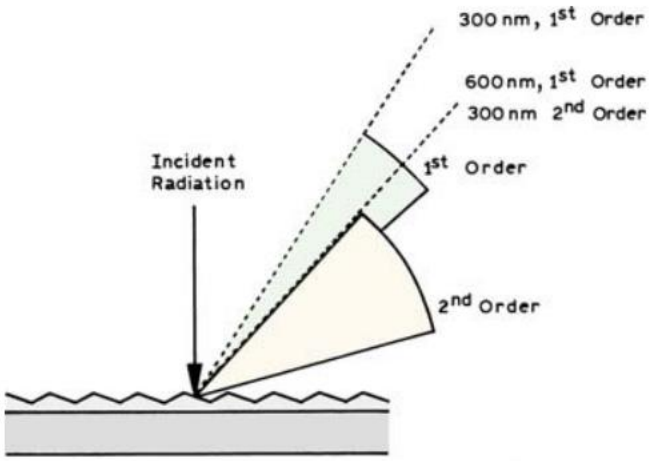

Figure 3.1b: Reflection grating exhibiting diffraction of light on grating surface.[2]

To prevent the presence of this instrumental source of interference, the range of the wavelengths of the emission spectra should be kept to less than twice the wavelength of the excitation wavelength. Also, high-pass or low-pass filters can be used to remove undesired light from higher-order diffraction.

The final, and perhaps most troubling source of interference experienced in these photoluminescence studies resulted from Raman scattering in the sample solvents. An example spectrum of Raman scattering in dichloromethane is shown in **Figure 3.1c**.

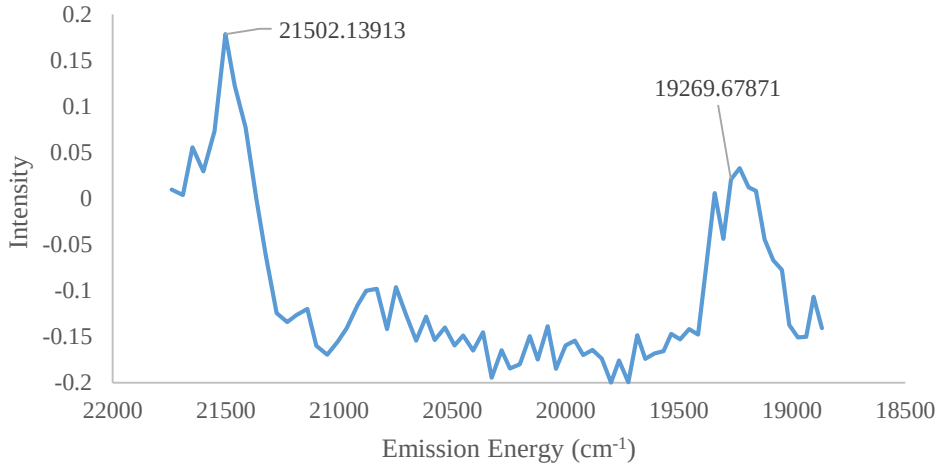

Figure 3.1c: Raman scattering measured in fluorescence emission spectrum taken in dichloromethane corresponding to excitation energy of 22,222 cm^{-1}.

Such scattering was particularly misleading as the peaks are unambiguous and exhibit Stokes shifts with magnitudes similar to those expected for the fluorescence emission peaks of the gold(I) complexes. Additionally, the presence of multiple scattering peaks was deceptive as multiple emissions were anticipated for these azulenylthiolate gold(I) complexes. However, there exist several indications that these peaks were due to scattering rather than fluorescence.

Firstly, regardless of the energy of the excitation wavelength, the scattering peaks randomly fluctuated around an average Stokes shift of 3053 cm^{-1} lower in energy than the energy of the excitation. **Figure 3.1d** shows the observed Stokes shifts for Raman scattering in CH_2Cl_2. Unlike fluorescence and phosphorescence emissions, the Stokes shift of Raman scattered light does not depend on the energy of the incident light. If the incident light exceeded 25,000 cm^{-1}, a secondary scattering peak averaging a Stokes shift of 752 cm^{-1} was also observed. Again, the

Stokes shift of this secondary scattering peak was independent of the energy of the incident radiation.

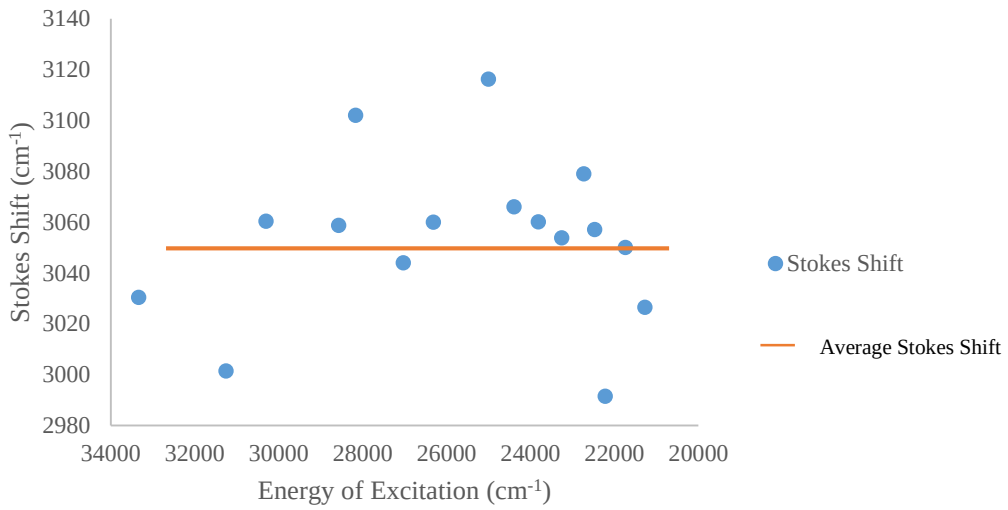

Figure 3.1d: Stokes shifts of Raman scattering in dichloromethane & average Stokes shift.

The second indication that the peaks in these spectra arise from Raman scattering rather than fluorescence is that the magnitude of the intensities of the peaks is significantly less than the magnitude typical for emission from fluorescence or phosphorescence; the intensity of fluorescence should be about two orders of magnitude greater than the peaks seen in **Figure 3.1c**. Raman scattering was also observed in liquid 2-methyl THF with an average Stokes shift of 2925 cm^{-1}. Because Raman scattering is much less intense than fluorescence, the two should be distinguishable in an emission spectrum. No high-intensity peaks were seen in the room-temperature fluorescence studies of the mercaptoazulene ligands or their gold(I) complexes due to quenching of fluorescence through the excited species' collisions with solvent molecules. Therefore, all luminescence studies were performed at 77K in 2-methly THF to reduce external conversion relaxation pathways.

3.2 Electronic & Photoluminescent Profiles of Several Azulenylthiolate Gold(I) Complexes

Once the origins of the sources of interference were identified, characterizing the photoluminescence profiles of several of the free ligands and their gold(I) complexes was undertaken. **Figure 3.2a** and **Figure 3.2b** provide two examples of comparative absorption spectra of the mercaptoazulene free ligand versus their respective gold(I) complexes. To obtain both the ultraviolet and the visible absorption profiles, the spectrophotometer must switch between visible and UV light sources. The distinct difference in the resolution of the visible and ultraviolet absorption profiles for 2.2c indicates that likely the xenon flash lamp that produces UV radiation was faulty, which may have in turn affected absorbance measurements and led to the meaningless negative molar absorptivities shown in the spectrum of 2.2c. Although the molar absorptivities are not accurate for 2.2c, **Figure 3.2a** still serves as a useful tool for comparison of the respective peaks for the free ligand and its gold(I) complex.

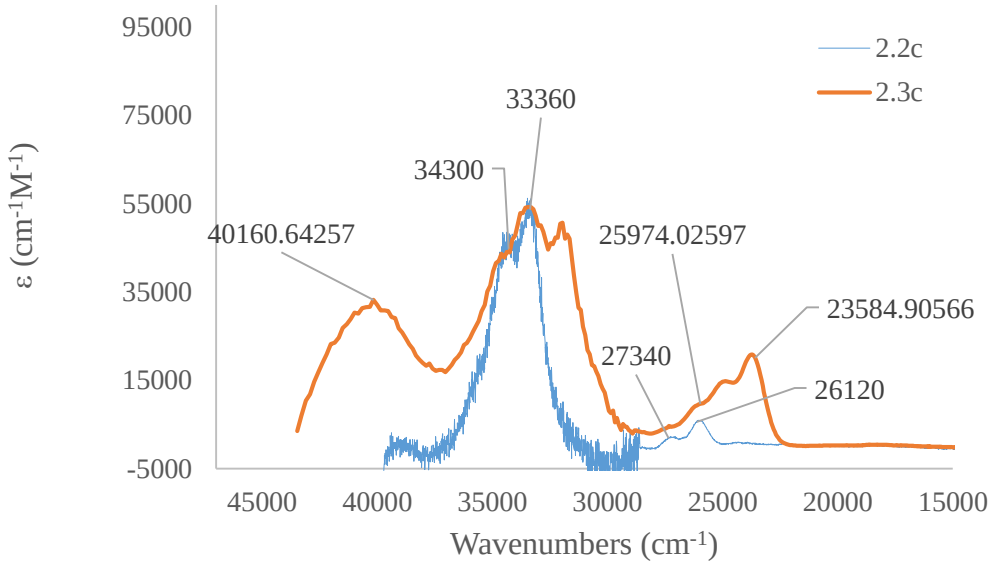

Figure 3.2a: Absorption spectra for free ligand and complex, 2.2c (blue) and 2.3c (orange), respectively.

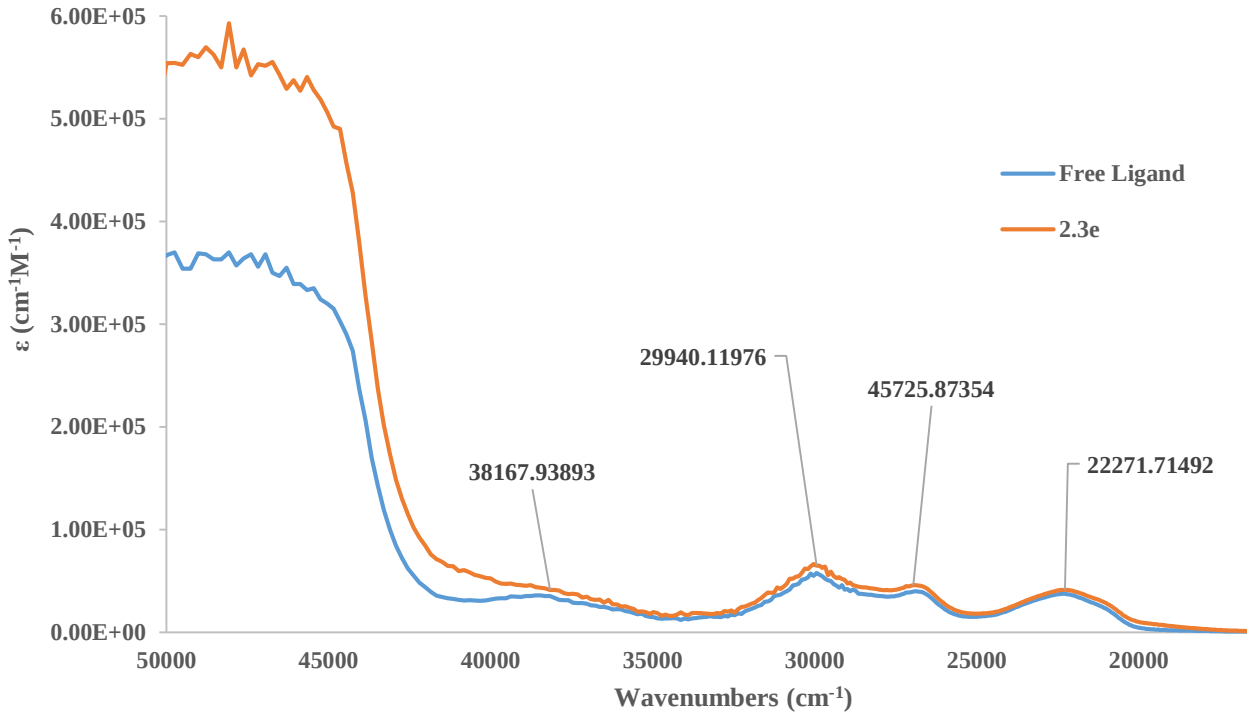

Figure 3.2b: UV-vis spectra of 2.3e (orange) and its precursor free ligand (blue)

In both **Figure 3.2a** and **Figure 3.2b**, it is notable that nearly all transitions appear stronger, even if only slightly, for the gold(I) complexes versus their respective free ligands. Additionally, in both figures, the high-energy transitions at energies of 40,000 cm^{-1} and higher are much more intense for the gold(I) complexes, likely due to overlapping $\pi \rightarrow \pi^*$ transitions from the PPh_3 groups.

To probe the emissive behavior of these species, the excitation wavelength was set to match the energy of the local maxima within each absorption spectra. Then, the peaks in the emission spectra were identified and an excitation scan was run to determine the wavelengths of light that most strongly correlate with each emission. This iterative process was performed until the peaks

in both the emission and excitation spectra were resolved to the highest possible resolution. The fluorescence emission/excitation spectra across the region of UV-vis absorption for **2.3c** are shown in **Figure 3.2c** on the next page.

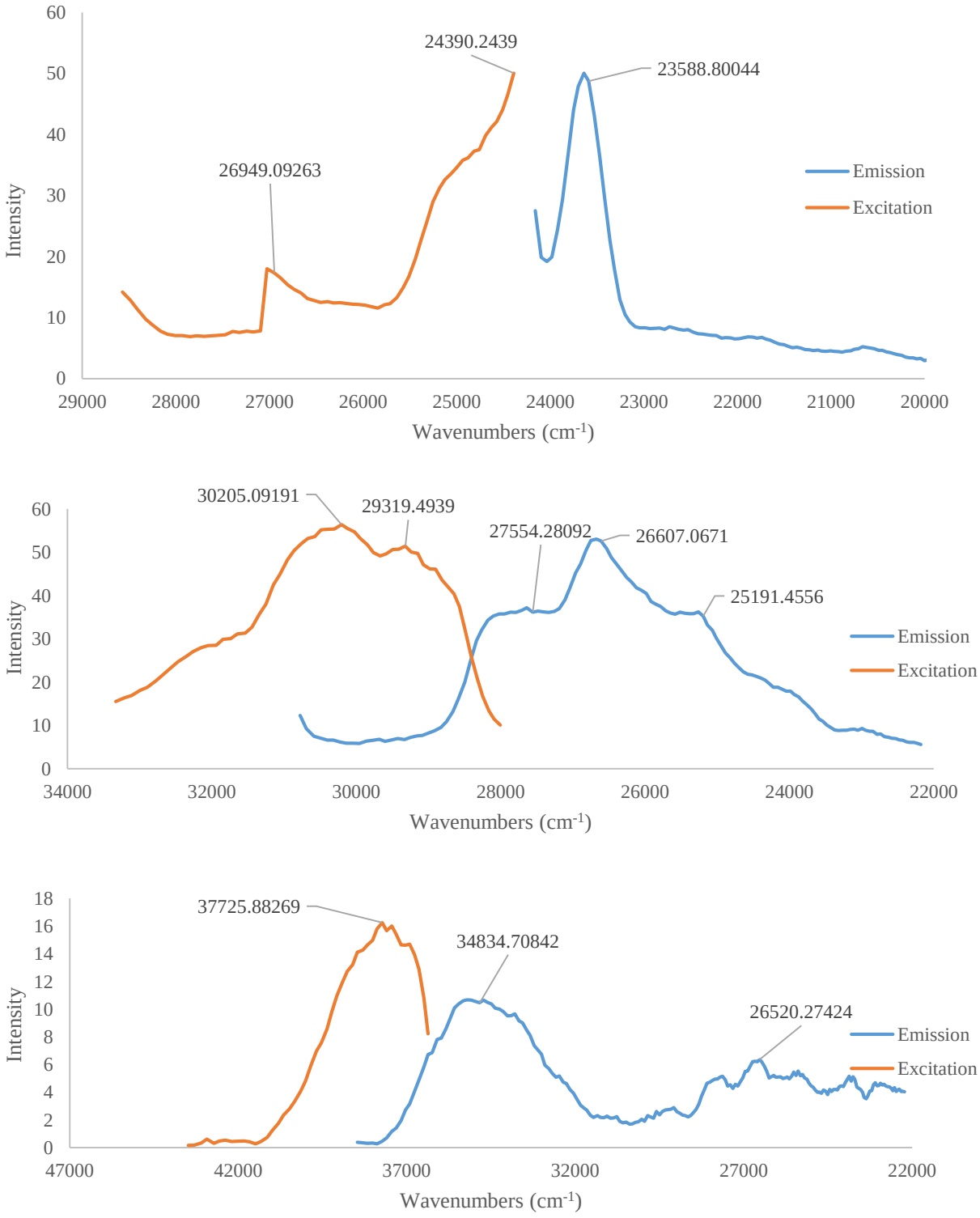

Figure 3.2c: Fluorescence excitation (orange) and emission (blue) across the UV-vis absorption region of complex 2.3c. Note that emissive behavior does indeed occur across the entire region of absorption and multiple emissions were observed for the bottom two spectra.

As seen in **Figure 3.2c**, complex **2.3c**, 2-azulenylthiolate gold(I) triphenylphosphine, displays highly fluorescent behavior. These spectra highlight its emissive behavior across its entire range of absorption within the UV-visible region. Additionally, the higher-energy excitations at 30205 cm^{-1} and 37725 cm^{-1} produced spectra containing multiple, broad emission bands. Furthermore, the spectra in **Figure 3.2d** display the phosphorescence profile of **2.3c**. The relative intensities of the phosphorescence emission peaks were less than that of the fluorescence emissions, as expected. Additionally, the Stokes shifts displayed in these spectra are greater than the Stokes shift for fluorescence, which is a result of energy loss through intersystem crossing.

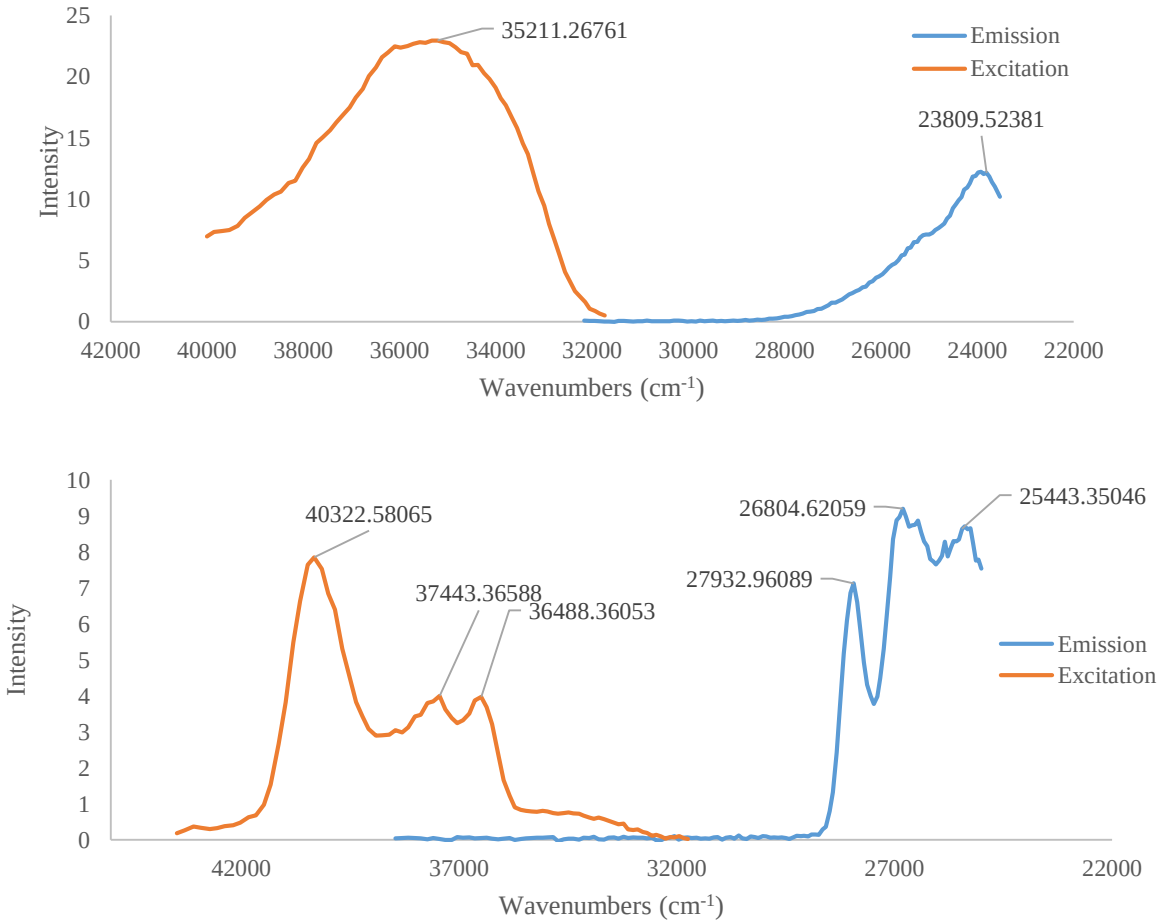

Figure 3.2d: Phosphorescence spectra of 2.3e; note the lesser intensity of the emission peaks compared to fluorescence, as well as the relatively large Stokes separation between emission and excitation bands.

Very similar spectral patterns were observed in the fluorescence studies of **2.3e**, the biazulenic system. Several of the experimental fluorescence spectra of **2.3e** are shown below in **Figure 3.2e**.

Figure 3.2e: Fluorescence spectra of 2.3e show emissive behavior at several regions within the UV-vis region. Note the similarity in shape of the bottom emission spectrum and the second emission spectrum in Figure 3.2c.

The emissive properties of all of the gold(I) complexes covered in Chapter 2 have yet to be catalogued. However, all of these complexes are expected to exhibit highly active photoluminescence profiles. Crystallographic data and time-dependent density functional theory (TD-DFT) were employed to help assign the electronic transitions that correspond to the peaks

seen in several of the above photoluminescence and electronic spectra. Interpretation of these results will be discussed in the following chapter.

Chapter 3 References:

[1] Neal, B. M.; Vorushilov, A. S.; DeLaRosa, A. M.; Robinson, R. E.; Berrie, C. L.; Barybin, M. V.; *"Ancillary Nitrile Substituents as Convenient IR Spectroscopic Reporters for Self-Assembly of Mercapto- and Isocyanoazulenes on Au(111),"* Chemical Communications, **2011**, 47, 10803-10805.

[2] Lakowicz, J.R.; *"Principles of Fluorescence Spectroscopy,"* Springer Publishing Co., **2006**, 27-60.

[3] Skoog, D.; Holler, J.F.; Crouch, S.R.; *"Principles of Instrumental Analysis,"* Thomson Brooks/Cole, **2007**, 180-182.

Chapter 4:

X-ray Crystal Structures & Interpretation of Electronic & Photoluminescence Spectra

4.1 Interpreting Electronic and Luminescence Spectroscopies

4.1a *Assessing the Effect of Aurophilic Interactions on the Electronic & Luminescence Spectra via X-ray Crystallography*

As addressed in Chapter 1, aurophilic interactions can complicate the electronic and luminescence profiles of complexes containing gold(I) by introducing LMMCT relaxation pathways between gold centers. Given that **2.3c** and **2.3e** displayed extensive absorption within the UV-vis region, as well as emissions across the expanse of their absorption profiles, it was important to consider aurophilic interactions as potential origins for some of the observed emissive behavior. The ensuing discussion will provide an overview of some of the key structural parameters of complexes **2.3c** and **2.3e** that shed light on the possibility for these complexes to exhibit emissions from LMMCT relaxation pathways.

In optimizing the synthesis of **2.3c**, crystals were successfully grown and were analyzed via single-crystal X-ray crystallography by Dr. Nikolay Gerasimchuk at Missouri State University. The resulting X-ray crystal is shown below in **Figure 4.1a**.

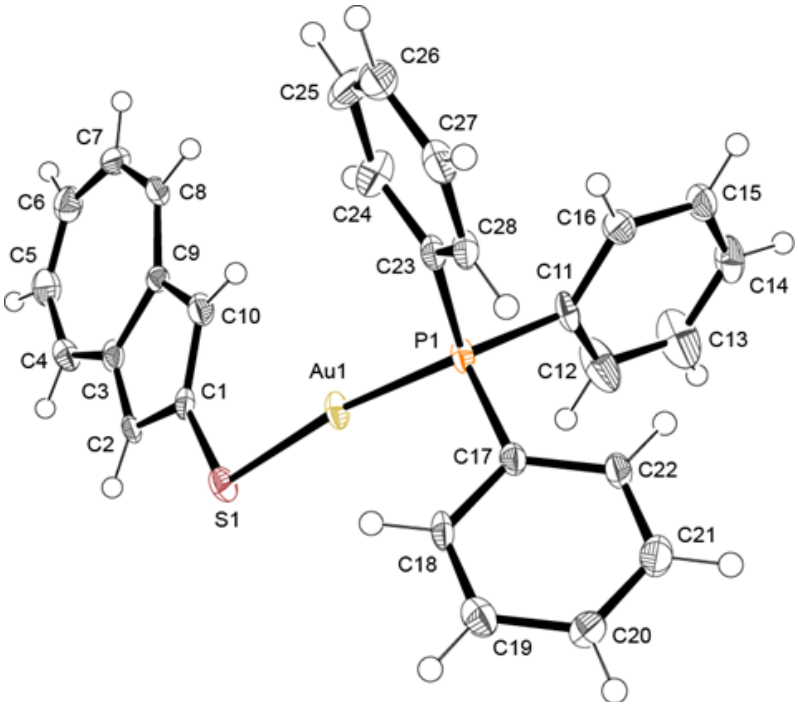

Figure 4.1a: X-ray crystal structure of 2-azulenylthiolate gold(I) triphenylphosphine (50% thermal ellipsoids).

The Au-S bond length is approximately 2.301 Å while the Au-P bond is slightly shorter at 2.2624 Å. Both of these bond lengths are similar to corresponding typical bond distances observed in benzenoid PPh_3-gold(I)-thiolate systems.[1] Also similar to related complexes is the nearly linear S-Au-P bond angle at 171.71º. The linear S-Au-P unit and the plane of defined by azulene backbone are practically co-planar, separated by a mere 11º. This dihedral angle is less than that of the congener of **2.3c** with ethoxycarbonyl substituents at the 1 and 3 positions which push the (PPh_3)Au unit out of the azulenic plane. Perhaps most significantly, the bulky phenyl rings cause all intermolecular Au-Au distances to be greater than 3.3 Å, which is the maximum Au-Au separation at which aurophilic interactions can take place.[2] Therefore, **2.3c** should not have accessible aurophilic charge transfer pathways.

Crystals of **2.3e** were first synthesized by Dr. Andrew Spaeth and the crystal structure was determined again with help from Dr. Nikolay Gerasimchuk. Notably, the biazulene framework is

planar, which should allow for electronic delocalization across the entire ligand. The Au-S and Au-P bond lengths are essentially identical to those found for **2.3c**. Interestingly, the S-Au-P unit is more linear than that of **2.3c** at 174.29º. Perhaps the bulky ethoxycarbonyl substituents sterically repel the gold(I) center away from the azulenic scaffold and further in line with sulfur and phosphorous. The dihedral angle between the S-Au-P unit and the azulenic scaffold was, as expected, about 15.7º. Since the coordination sphere immediately surrounding the gold(I) center is similar to that of **2.3c**, aurophilic interactions are not expected due to the interfering, bulky PPh_3 ligands.

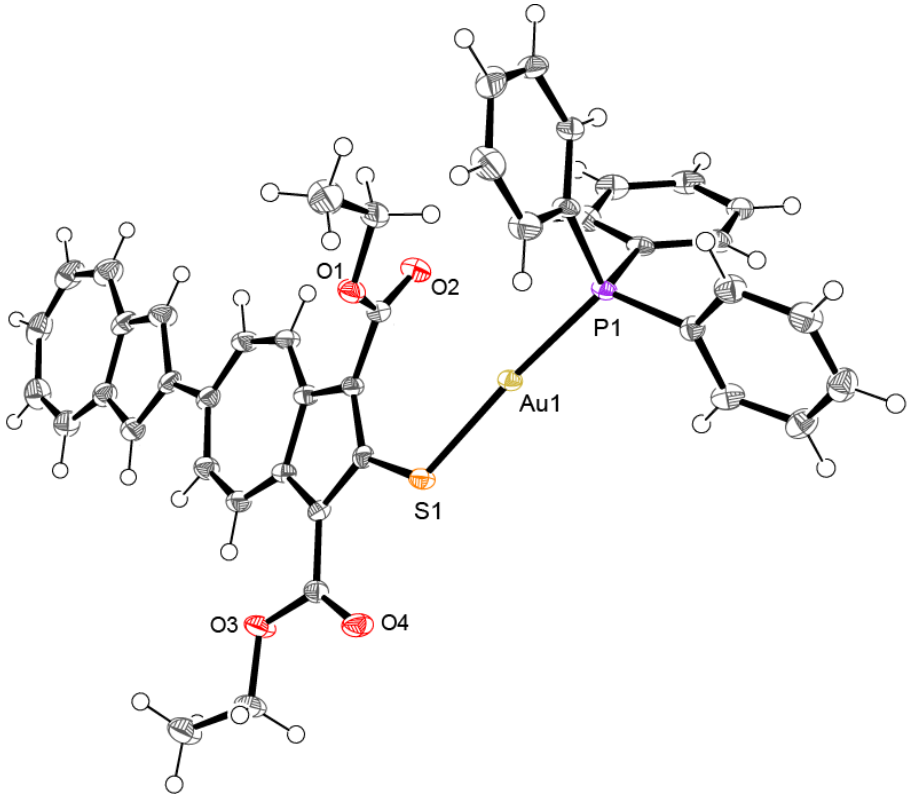

Figure 4.1b: X-ray crystal structure 2.3e (50% thermal ellipsoids).

4.2 *TD-DFT Studies for Interpretation of Electronic & Luminescence Spectra*

Ruling out the potential for electronic transitions complicated by aurophilic interactions, with the help of Nate Erickson, TD-DFT was employed to aid in the assignment of the specific electronic transitions that correspond to the absorption and emission profiles of these species. The BP86 functional with a TZVP basis set was used to calculate the optimal geometry of the structure for **2.3e** in the gas phase. Then a calculation using a TPSSh functional with a TZVP basis set was run to generate orbital densities of different electronic states and a theoretical absorption spectrum. **Figure 4.2a** shows the theoretical absorption spectrum superimposed over the experimentally obtained spectrum for species **2.3e**.

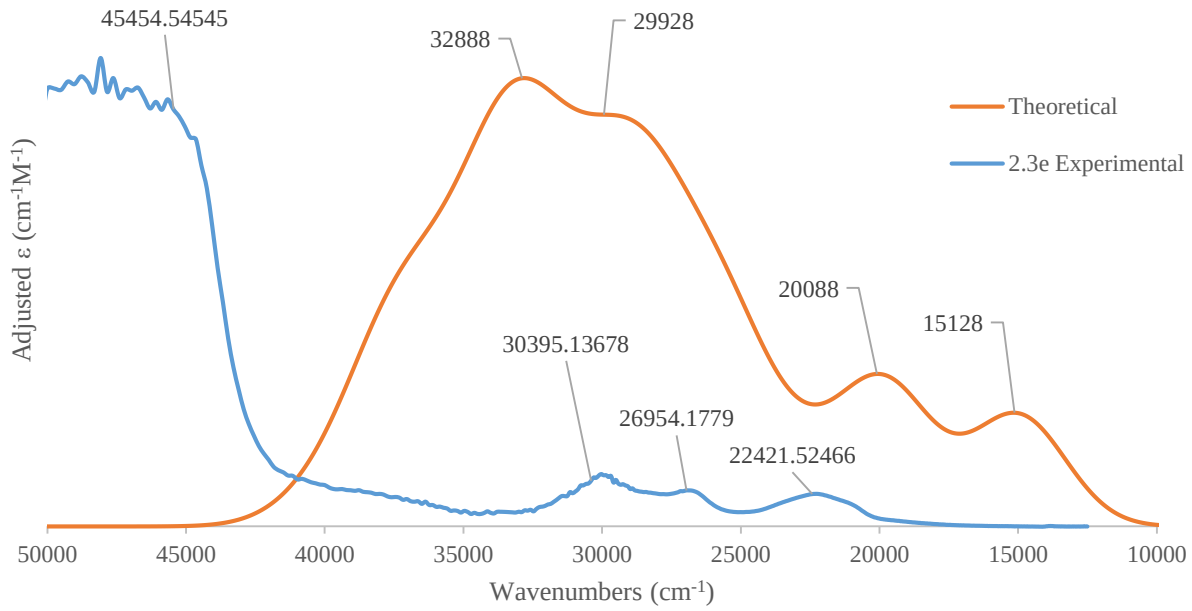

Figure 4.2a: Theoretical absorption spectrum of 2.3e (orange); experimental absorption spectrum (blue).

Although the theoretically determined spectrum is shifted to lower energy, it correctly predicts the number of charge transfer bands seen experimentally, as well as the trend in their respective intensities. This is particularly helpful, as each of the bands in the theoretical spectrum

can be traced back to excitations between specific molecular orbitals. It is known that most of the luminescent properties of phosphinegold(I) thiolates originate from charge transfers of the lone pair on sulfur to the ligand or the metal center (LLCT or LMCT).[3] Therefore, thiolate-to-azulene or thiolate-to-gold charge transfers were anticipated for **2.3e**. **Figure 4.2b** shows the theoretical absorption spectrum labeled with the major electronic transitions that are associated with each band, while **Figure 4.3b** illustrates the calculated orbital densities relevant to each electronic transition present in the electronic absorption spectrum.

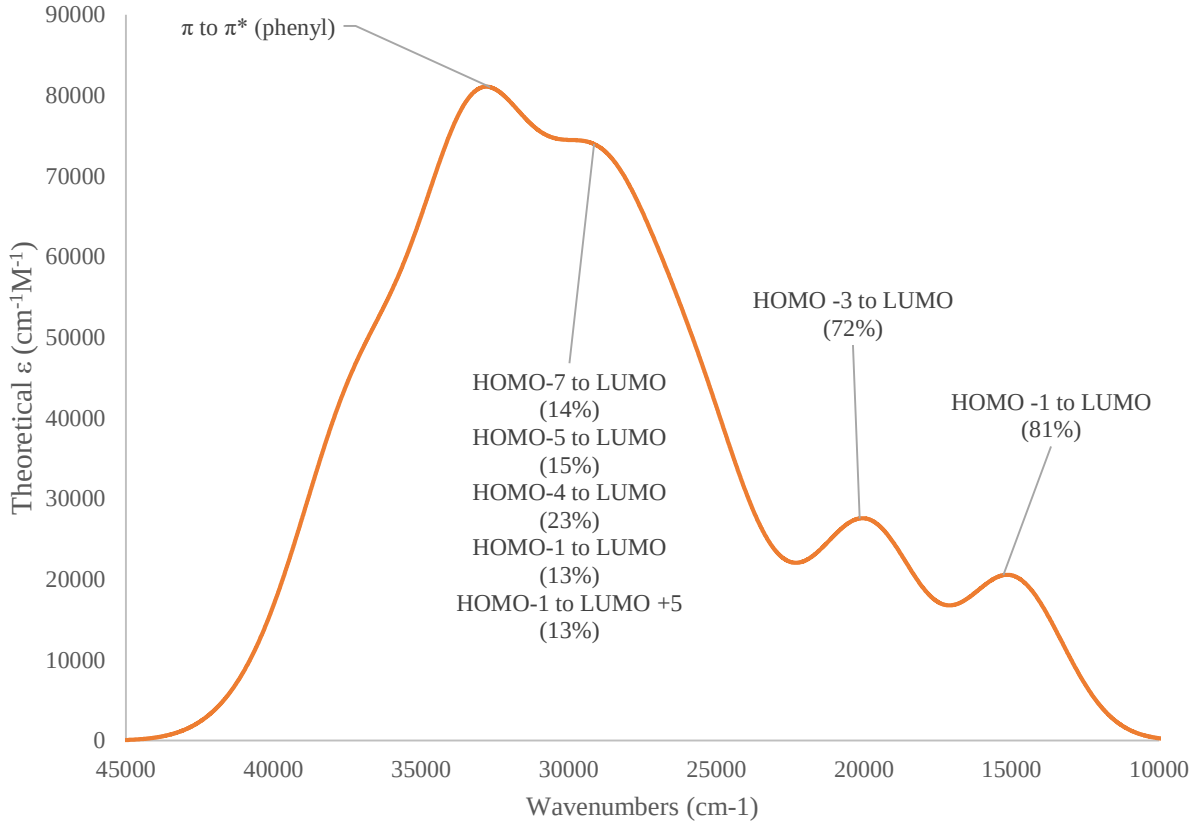

Figure 4.2b: Theoretical absorption spectrum of 2.3e labeled with specific electronic transitions.

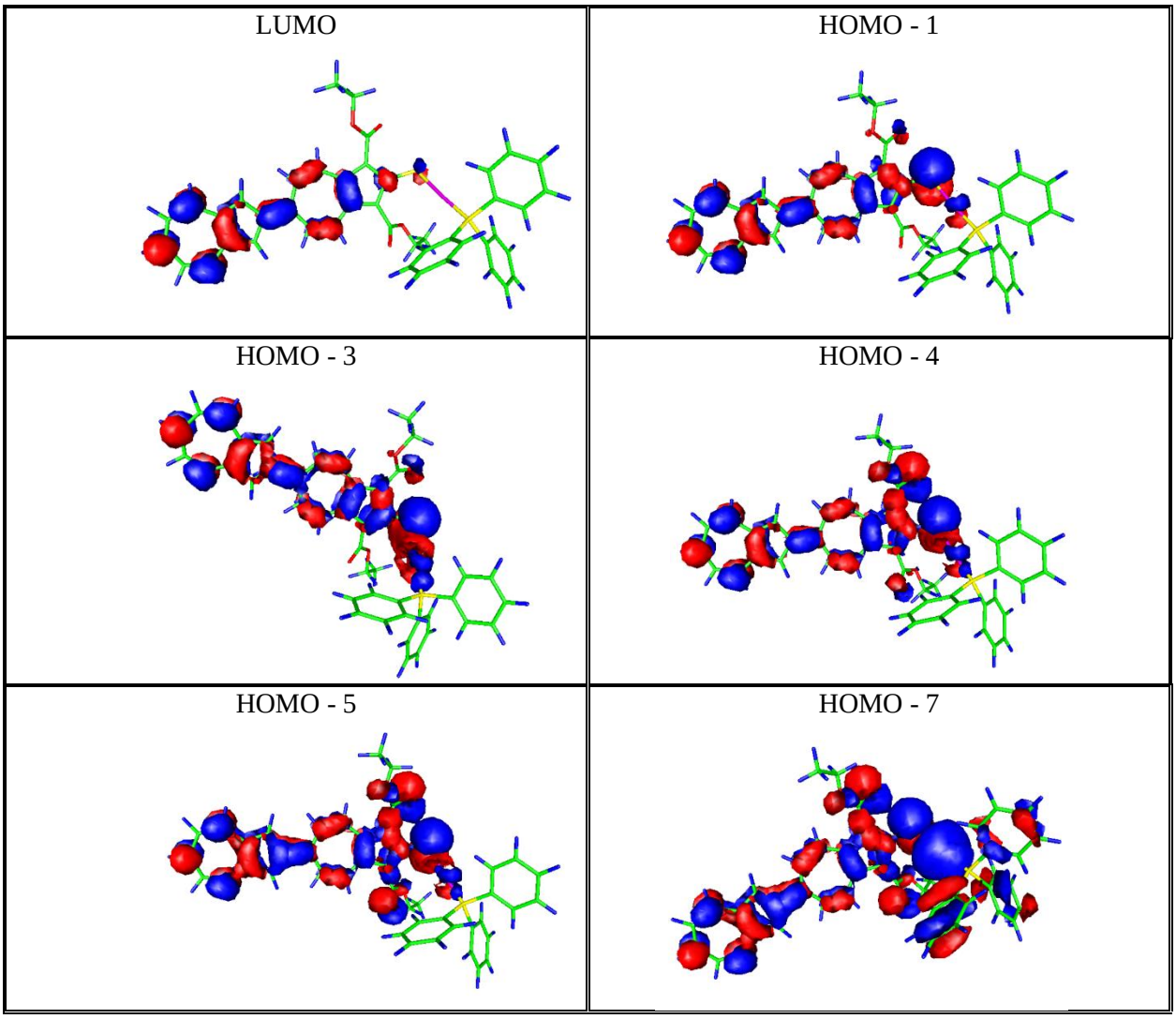

Figure 4.2c: TD-DFT-calculated orbital densities of molecular orbitals corresponding to charge transfer bands labeled in Figure 4.2b.

From **Figure 4.2b** and **Figure 4.2c**, it can be determined that the low-energy HOMO – 1 → LUMO transition may be assigned as sulfur-to-azulene charge transfer. The HOMO – 1 has significant orbital density on sulfur which diminishes significantly in the LUMO as charge density is delocalized across the entire biazulene backbone. Indeed, other than the reduced orbital density on the thiolate, the only orbitals open to accept an excited electron in the LUMO reside on the azulenic framework. The three lowest-energy transitions labeled in **Figure 4.2b** involve the HOMO – 3, HOMO – 4, and HOMO – 5, which display charge density both gold and sulfur.

Therefore, transitions from these orbitals potentially represent thiolate-to-azulene charge transfers (LLCT) and gold-to-azulene charge transfers (MLCT). The HOMO – 7 orbital has significant orbital density on the phenyl rings, indicating a $\pi \rightarrow \pi^*$ transition from the phenyl substituents to the LUMO of azulene. Such $\pi \rightarrow \pi^*$ transitions from the phenyl groups are the origin of the highest-energy transition as well. It is also important to note that all of the populated states display significant electron density across the azulenic framework, which leads to $\pi \rightarrow \pi^*$ transitions from these states to the LUMO. These transitions overlap with the other charge transfer transitions in the theoretical electronic absorption profile, complicating the assignment of each band in the spectrum. To better visualize the electron-transfer mechanisms which give rise to the electronic transitions illustrated in **Figure 4.2b**, further TD-DFT electron-density difference maps will be plotted for the populated and excited states of species **2.3e**.

Assigning the transitions in the absorption spectrum of **2.3e** allows for the determination of the electronic states involved in the excitation and emission spectra shown in **Figure 3.2e**. By superimposing the experimental UV-vis spectrum over the experimental fluorescence spectra, the transitions associated with each emission and excitation peak become clearer, as shown in **Figure 4.2d**.

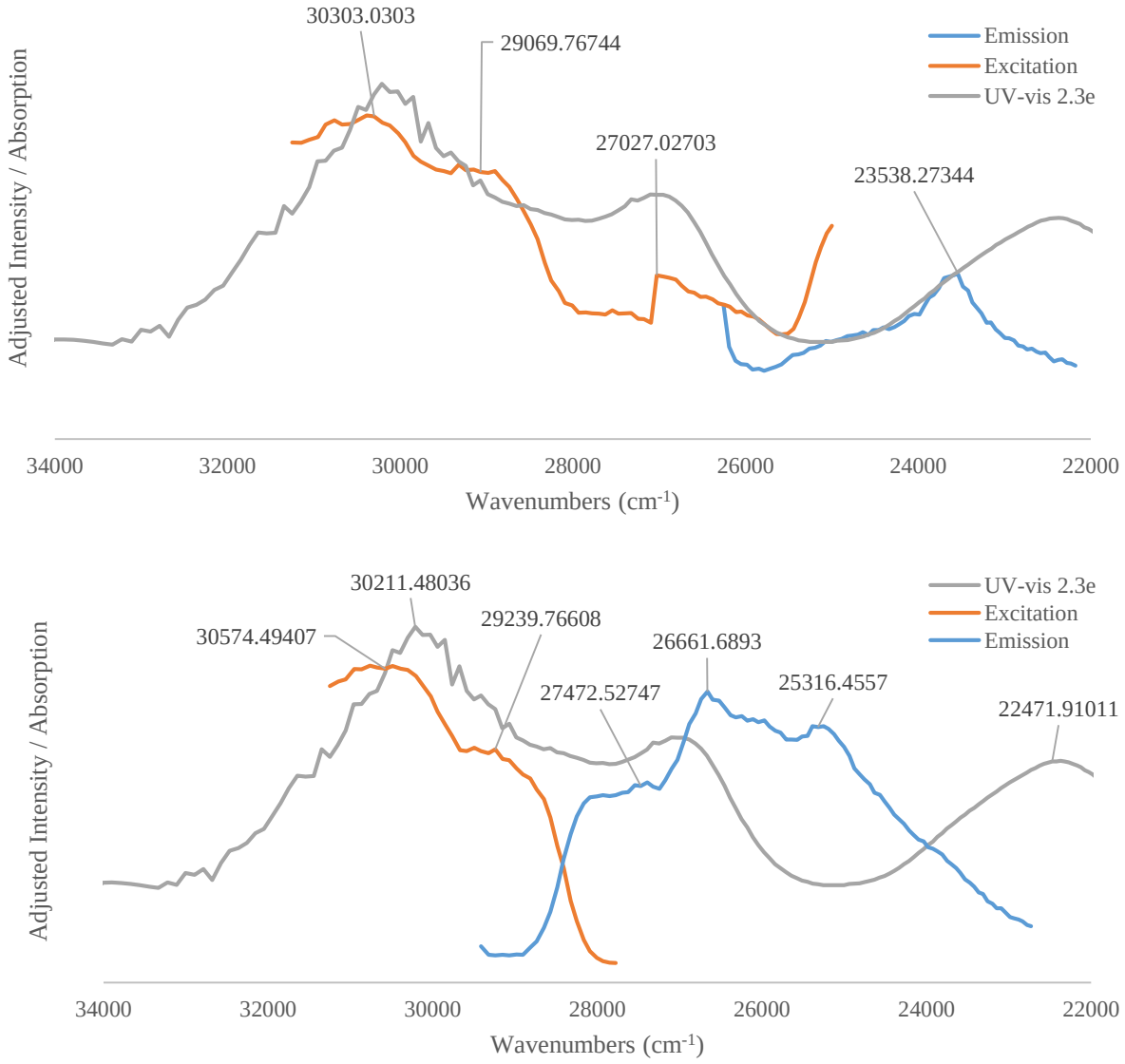

Figure 4.2d: superimposed UV-vis and fluorescence spectra of 2.3e.

Applying the transition information shown in **Figure 4.2b** to the above spectra elucidates the origins of excitation and emission peaks. It is clear that excitations around 30,000 cm^{-1}, which correspond to transitions from the HOMO – 1, HOMO – 4, HOMO – 5, and HOMO – 7 to the LUMO, produce broad emission spectra. The top spectra in **Figure 4.2d** shows that an emission peak occurs within the lowest-energy band of the UV-vis spectrum, which represents relaxation via azulene-to-thiolate charge transfer from the LUMO→HOMO – 1. Interestingly, more intense emission occurs at higher energies between 28,000 cm^{-1} and 25,000 cm^{-1}, which is associated with

a LUMO→HOMO – 3 transition, which may be azulene-to-thiolate (LLCT) or azulenylthiolate-to-gold charge transfer (LMCT). Notably, although the expected MLCT and LLCT bands were observed and this biazulenylthiolate gold(I) system exhibits multiple emissions within the UV-vis region, it does not break Kasha's rule as all observed emissions occur from the LUMO.

Figure 3.2c illustrates that the 2-azulenylthiolate gold(I) system exhibits similar emissive behavior to **2.3e**. The fluorescence spectra contains a single lower-energy peak and several broad higher-energy emissions that resemble the LLCT and LMCT bands of the biazulenic system. Thus, these bands can tentatively be assigned as azulene-to-thiolate charge transfer and azulenylthiolate-to-gold charge transfer, respectively. In order to confirm these conjectures, further TD-DFT studies are necessary.

Benzenoid phosphinegold(I) thiolate systems often exhibit LMCT emission bands at energies between 14,245 cm^{-1} and 24,213 cm^{-1}.[4] In this case, the LMCTs of the biazulene system were primarily higher in energy than those observed for benzenoid systems. The LMCT bands occur only for the higher energy transitions involving the HOMO – 3, HOMO – 4, HOMO – 5, and HOMO – 7 orbitals. As shown in **Figure 4.2c**, all of these states have significant orbital density across the entire azulenic scaffold, on sulfur and gold, and on the ethoxycarbonyl substituents. Electron density on the thiolate is therefore delocalized across the entire system and is particularly affected by the electron-withdrawing nature of the ethoxycarbonyl substituents. This withdrawal of electron density from the thiolate is a stabilizing effect, causing the excitation of electrons from these states to be higher-energy transitions. Therefore, LMCT from the LUMO back to sulfur and gold should produce higher-energy emissions than do typical LMCT emissions in benzenoid systems. This blue-shifting of the emission spectra has been well-documented for a number of benzenoid systems containing electron withdrawing groups.[5]

Chapter 4 References:

[1] Nunokawa K.; Okazaki K.; Onaka S.; Ito M.; Sunahara T.; Ozeki T.; Imai H.; Inoue K.; "*Synthesis and X-ray structure study on new Au(I) polymer architectures based on multi-sulfur tentacles,"* J. Organometallic Chemistry, **2005**, 690, 1332–1339.

[2] Schmidbaur, Hubert; *"The Aurophilicity Phenomenon: A Decade of Experimental Findings, Theoretical Concepts and Emerging Applications,"* Gold Bulletin, **2000**, 33, 3-10.

[3] Tiekinka E. R.T.; Kang, J.G; *"Luminescence properties of phosphinegold(I) halides and thiolates,"* Coord. Chem. Rev., **2009**, 253, 1627–1648.

[4] Yam, W.W.V.; Chan, C.L.; Li, C.K.; Wong, K.M.C.; *"Molecular design of luminescent dinuclear gold(I) thiolate complexes; from fundamentals to chemosensing,"* Coord. Chem. Rev., **2001**, 216-217, 173-194.

[5] Forward J.M.; Bohmann D.; Fackler, J.P.; Staples, R.J.; "*Luminescence Studies of Gold(1) Thiolate Complexes,"* Inorganic Chemistry, **1995**, Vol. 34, 6330 – 6336.

Chapter 5:

Conclusions & Future Work

5.1: Conclusions & Future Work

The work presented herein provides a holistic approach to the synthesis and characterization of a family of azulenylthiolate gold(I) complexes. Firstly, it was shown by following the purification of 2-azulenylthiolate gold(I) triphenylphosphine through ^{1}H NMR that the protonation of this species is more kinetically favorable than its congener with ethoxycarbonyl substituents. Additionally, it was known that azulenic systems and the phosphinegold(I) thiolate motif could exhibit unique photoluminescence properties. This potential for intriguing photoluminescence profiles motivated the study of the emissive behavior of these azulenylthiolate gold(I) complexes. After removing possible sources of spectral interference, it was shown experimentally that several of these complexes manifest complex fluorescence and phosphorescence profiles. Crystallographic data revealed that aurophilic effects would not complicate the luminescence spectra of these species as the bulky triphenylphosphine ligands introduced steric repulsions between gold(I) centers. Still, rich fluorescence and phosphorescence profiles were obtained that exhibited emissions across much of the UV-vis spectrum. The origins of the excitations/emissions were assigned for species **2.3e** and tentatively for **2.3c** through TD-DFT.

Coupling experimental photoluminescence studies with computational results confirmed that the gold(I) complexes comply with trends seen in similar systems, namely that the lowest-energy emission consists of a azulene-to-thiolate charge transfer and that the higher-energy emissions are likely comprised of several LMCT transitions. The observed transitions were higher in energy than analogous benzenoid systems due to the electron-withdrawing ethoxycarbonyl substituents that reduce electron density on the thiolate. These systems did not appear to break Kasha's Rule, exhibiting emission from only the lowest-energy excited state.

To continue the studies of this family of azulenylthiolate gold(I) complexes, the fluorescence and phosphorescence profiles of the remaining complexes will be catalogued. Solid-state photoluminescence studies could provide further insight into the emissive behavior of these systems by providing improved resolution and elimination of sources of interference from the solvent. Additionally, further TD-DFT studies, including the plotting of electron-density difference maps, will be conducted to qualitatively assign the electronic transitions associated with the emission and excitation spectra of the remaining gold(I) complexes. Once fully characterized, it is possible that these azulenylthiolate gold(I) systems may serve as viable, relatively non-toxic systems for luminescent chemosensing applications.